Inorg. Chem. **2007**, *46*, 8332–8348

Sulfur X-ray Absorption and Vibrational Spectroscopic Study of Sulfur Dioxide, Sulfite, and Sulfonate Solutions and of the Substituted Sulfonate Ions $X_3CSO_3^-$ (X = H, Cl, F)

Emiliana Damian Risberg,[†] Lars Eriksson,[†] János Mink,[‡] Lars G. M. Pettersson,[§] Mikhail Yu. Skripkin,[||] and Magnus Sandström*,[†]

Department of Physical, Inorganic and Structural Chemistry, Stockholm University, SE-106 91 Stockholm, Sweden, Department of Molecular Spectroscopy, Chemical Research Center of the Hungarian Academy of Sciences, P.O. Box 77, H-1525 Budapest, Hungary, Faculty of Information Technology, Research Institute of Chemical and Process Engineering, University of Pannonia, P.O. Box 158, H-8201 Veszprém, Hungary, Department of Physics, AlbaNova, Stockholm University, SE-106 91 Stockholm, Sweden, and Department of Chemistry, Saint-Petersburg State University, Universitetsky pr. 26, 198504 Saint-Petersburg, Russia

Received December 20, 2006

Sulfur K-edge X-ray absorption near-edge structure (XANES) spectra have been recorded and the S(1s) electron excitations evaluated by means of density functional theory–transition potential (DFT–TP) calculations to provide insight into the coordination, bonding, and electronic structure. The XANES spectra for the various species in sulfur dioxide and aqueous sodium sulfite solutions show considerable differences at different pH values in the environmentally important sulfite(IV) system. In strongly acidic (pH < ∼1) aqueous sulfite solution the XANES spectra confirm that the hydrated sulfur dioxide molecule, SO_2(aq), dominates. The theoretical spectra are consistent with an OSO angle of ∼119° in gas phase and acetonitrile solution, while in aqueous solution hydrogen bonding reduces the angle to ∼116°. The hydration affects the XANES spectra also for the sulfite ion, SO_3^{2-}. At intermediate pH (∼4) the two coordination isomers, the sulfonate (HSO_3^-) and hydrogen sulfite (SO_3H^-) ions with the hydrogen atom coordinated to sulfur and oxygen, respectively, could be distinguished with the ratio HSO_3^-:SO_3H^- about 0.28:0.72 at 298 K. The relative amount of HSO_3^- increased with increasing temperature in the investigated range from 275 to 343 K. XANES spectra of sulfonate, methanesulfonate, trichloromethanesulfonate, and trifluoromethanesulfonate compounds, all with closely similar S–O bond distances in tetrahedral configuration around the sulfur atom, were interpreted by DFT–TP computations. The energy of their main electronic transition from the sulfur K-shell is about 2478 eV. The additional absorption features are similar when a hydrogen atom or an electron-donating methyl group is bonded to the $-SO_3$ group. Significant changes occur for the electronegative trichloromethyl (Cl_3C–) and trifluoromethyl (F_3C–) groups, which strongly affect the distribution especially of the π electrons around the sulfur atom. The S–D bond distance 1.38(2) Å was obtained for the deuterated sulfonate (DSO_3^-) ion by Rietveld analysis of neutron powder diffraction data of $CsDSO_3$. Raman and infrared absorption spectra of the $CsHSO_3$, $CsDSO_3$, H_3CSO_3Na, and $Cl_3CSO_3Na{\cdot}H_2O$ compounds and Raman spectra of the sulfite solutions have been interpreted by normal coordinate calculations. The C–S stretching force constant for the trichloromethanesulfonate ion obtains an anomalously low value due to steric repulsion between the Cl_3C– and $-SO_3$ groups. The S–O stretching force constants were correlated with corresponding S–O bond distances for several oxosulfur species.

Introduction

Acid−base reactions in aqueous solutions of sulfur dioxide are of great importance in environmental and atmospheric chemistry and in the global sulfur cycle.[1] The availability of sulfur 3d orbitals promotes covalency in the sulfur−oxygen bonds, and a variety of sulfite(IV) species can form in acidic aqueous solutions, despite the apparent simplicity of the SO_2/H_2O system.[2] Very few spectroscopic methods can favorably be applied to study structure and speciation

* To whom correspondence should be addressed. E-mail: magnuss@struc.su.se.
[†] Department of Physical, Inorganic and Structural Chemistry, Stockholm University.
[‡] University of Pannonia.
[§] Department of Physics, AlbaNova, Stockholm University,
[||] Department of Chemistry, Saint-Petersburg State University.

(1) Granat, L.; Rodhe, H.; Hallberg, R. O. *Ecol. Bull.* **1976**, *22*, 89−134 (Nitrogen, Nitrogen Sulphur-Global Cycles).

10.1021/ic062440i CCC: $37.00
Published on Web 09/05/2007

of sulfur species in dilute solution. Recently, sulfur K-edge X-ray absorption near-edge structure (XANES) spectroscopy at dedicated synchrotron beamlines has developed into a sensitive and direct in situ method for such analyses and also for environmental samples which can be kept at atmospheric pressure of helium.[3]

The probability and energy of the dipole-allowed ($\Delta l = \pm 1$) electronic transitions of the sulfur 1s electron to unoccupied valence molecular orbitals with some 3p character can be greatly influenced by the bonding and chemical environment of the sulfur atom. As a first approximation, the ionization energy of the K-edge can be qualitatively correlated to the "effective" oxidation state in the sulfur species.[4] In addition, the XANES preedge features often contain several electronic transitions with an intensity reflecting the amount of S 3p character in the receiving unoccupied molecular orbital.[5] The composite band shape, which then depends on the probability and relative energy for each inherent S 1s transition and also is influenced by intermolecular interactions, carries information about the covalency and coordination geometry of the bonds to the sulfur atom.

The relative amount of different types of sulfur species in a sample can sometimes be evaluated semiquantitatively by fitting a linear combination of normalized standard XANES spectra to the experimental one.[3] For this purpose, it is important that the chemical environment of the characteristic sulfur groups in the standards is similar to that in the sample. XANES spectra can also be simulated theoretically, in particular the preedge part, by, e.g., density functional theory−transition potential (DFT−TP) computational methods by calculating the energy and probability of the dominating dipole-allowed ($\Delta l = \pm 1$) electronic transitions.[6] This is a useful method to assess how chemical interactions influence the spectral features of the sulfur groups, as has been demonstrated previously for some dimethyl sulfoxide complexes.[7] An alternative computational method is the treatment of core electron excitations by means of the relativistic two-component zero-order regular approximation (ZORA) and time-dependent density functional theory (TD-DFT) formalism.[8] This method has recently been applied on the S(1s) spectrum of the SO_2 molecule and allowed assignment of the main spectral features in the experimental spectrum. However, the computed absolute energies differ by about 25 eV from the experimental, even after a relativistic correction of about 8 eV.[8]

Horner and Connick investigated the aqueous sulfite system by means of ^{17}O NMR and studied the rate of oxygen exchange between sulfur(IV) species and water over a range of temperatures, pH, and concentrations.[9] In strongly acidic solutions molecular SO_2(aq) species were found to dominate. The first deprotonation of the hydrated SO_2(aq) molecule leads to a composite spectrum of two isomeric species in a temperature-dependent equilibrium, the hydrogen sulfite (SO_3H^-) and the sulfonate (HSO_3^-) ions.[9,10] The hydrogen atom is directly bonded to the sulfur atom in the sulfonate and to one of the oxygen atoms in the hydrogen sulfite ion.[9] The equilibrium quotient ($Q_d = [SO_3H^-]/[HSO_3^-]$) for the isomerization reaction has been reported as $Q_d = 4.9 \pm 0.1$ for solutions of ionic strength 1.0 m at 298 K.[9] For the sulfite and disulfite ($S_2O_5^{2-}$) ions their structure and equilibrium in aqueous solution have been studied by X-ray diffraction and Raman measurements.[11,12] With large cations it has been possible to isolate the sulfonate ion in the solid state.[13−15] Simon and co-workers studied the IR and Raman vibrational spectra of cesium and rubidium sulfonate salts already in 1960,[15] confirming C_{3v} symmetry for the sulfonate ion,[15,16] and later IR spectra of ammonium sulfonate were analyzed.[17] X-ray and neutron single-crystal structure studies have been performed of $CsHSO_3$, but the S−H distance remained uncertain.[13,14]

In this study, information has been obtained from both solution and solid-state studies. Rietveld analysis of neutron powder diffraction data of crystalline $CsDSO_3$ yielded the S−D distance, and normal coordinate methods were applied for a detailed force field analysis of IR and Raman spectra of $CsHSO_3$ and $CsDSO_3$. Sulfur K-edge XANES spectra have been recorded, also of a series of substituted sulfonate anions. The sensitivity of the sulfur 1s electron transitions to the chemical environment around the sulfur atom has been evaluated by DFT−TP methods, systematically comparing changes in the bonding character when replacing the sulfonate hydrogen atom with methyl (CH_3), trichloromethyl (CCl_3), or trifluoromethyl (CF_3) groups.

The methanesulfonate ($CH_3SO_3^-$) and trifluoromethanesulfonate ($CF_3SO_3^-$) anions are often used as counterions in organic solvents because of their weakly coordinating and

(2) Cotton, F. A.; Wilkinson, G.; Murillo, C. A.; Bochmann, M. *Advanced Inorganic Chemistry*, 6th ed.; John Wiley & Sons, Inc.: New York, 1999.

(3) (a) Fors, Y.; Sandström, M. *Chem. Soc. Rev.* **2006**, *35*, 399−415. (b) Sandström, M.; Jalilehvand, F.; Damian, E.; Fors, Y.; Gelius, U.; Jones, M.; Salomé, M. *Proc. Natl. Acad. Sci. U.S.A.* **2005**, *102*, 14165−14170. (c) Jalilehvand, F. *Chem. Soc. Rev.* **2006**, *35*, 1256−1268 and references therein.

(4) Vairavamurthy, A. *Spectrochim. Acta* **1998**, *A 54*, 2009−2017.

(5) (a) Stöhr, J. *NEXAFS spectroscopy*; Springer-Verlag: Berlin, 1992. (b) Solomon, E. I.; Hedman, B.; Hodgson, K. O.; Dey, A.; Szilagyi, R. K. *Coord. Chem. Rev.* **2005**, *249*, 97−129.

(6) (a) Triguero, L.; Pettersson, L. G. M.; Ågren, H. *Phys. Rev. B* **1998**, *58*, 8097−8110. (b) Slater, J. C. *Adv. Quantum Chem.* **1972**, *6*, 1−92. (c) Slater, J. C.; Johnson, K. H. *Phys. Rev. B* **1972**, *5*, 844−853.

(7) Damian, E.; Jalilehvand, F.; Abbasi, A.; Pettersson, L. G. M.; Sandström, M. *Phys. Scr.* **2005**, *T115*, 1077−1079.

(8) Fronzoni, G.; De Francesco, R.; Sterner, M.; Decleva, P. *J. Chem. Phys.* **2007**, *126*, 134308-1−134308-10.

(9) (a) Horner, D. A.; Connick, R. E. *Inorg. Chem.* **2003**, *42*, 1884−1894. (b) Horner, D. A.; Connick, R. E. *Inorg. Chem.* **1986**, *25*, 2414−2417.

(10) Voegele, A. F.; Tautermann, C. S.; Rauch, C.; Loerting, T.; Liedl, K. R. *J. Phys. Chem. A* **2004**, *108*, 3859−3864.

(11) Yamaguchi, T.; Lindqvist, O. *Acta Chem. Scand.* **1982**, *A36*, 377−389.

(12) Littlejohn, D.; Walton, S. A.; Chang, S.-G. *Appl. Spectrosc.* **1992**, *46*, 848−851.

(13) Johansson, L. G.; Lindqvist, O.; Vannerberg, N. G. *Acta Crystallogr.* **1980**, *B36*, 2523−2526.

(14) Johansson, L. G.; Lindqvist, O. *10 Nordiska Strukturkemistmötet, Program och Abstrakter*; Joulukuu: AM-International Oy, 1980; pp 88−89.

(15) Simon, A.; Schmidt, W. *Z. Electrochem.* **1960**, *64*, 737−741.

(16) Meyer, B.; Peter, L.; Shaskey-Rosenlund, C. *Spectrochim. Acta* **1979**, *A35*, 345−354.

(17) Hisatsune, I. C.; Heicklen, J. *Can. J. Chem.* **1975**, *53*, 2646−2656.

nonexplosive properties. In nucleophilic substitution reactions the trifluoromethanesulfonate ion is a good leaving entity, a property ascribed to the electronegative CF_3 group.[18−24] However, a recent ^{35}Cl nuclear quadrupole resonance study indicated the smallest coordinating ability for the trichloromethanesulfonate ($CCl_3SO_3^-$) ion.[25] Several analyses of the vibrational spectra of the anions above have been performed by normal coordinate analysis or quantum chemical calculations, despite the lack of structural data for trichloromethanesulfonate.[26−31] Numerous crystallographic studies have been carried out to structurally characterize methanesulfonate and trifluoromethanesulfonate compounds[32−40] but only one recently for the trichloromethanesulfonate ion.[41]

Experimental Details

Sample Preparation. The following chemicals were utilized: sulfur dioxide solution (SO_2 4.5−5.5% in water, Fluka); acetonitrile (CH_3CN, Riedel-de Haën); sodium sulfite (Na_2SO_3, 99.99%, Aldrich); cesium carbonate (Cs_2CO_3, 99.9%, Aldrich); deuterated water (D_2O, 99.9%, Larodan Fine Chemicals AB); trichloromethanesulfonyl chloride (CCl_3SO_2Cl, 97%, Aldrich); sodium methanesulfonate (CH_3SO_3Na, 98%, Alfa Aesar); sodium trifluoromethanesulfonate ($NaCF_3SO_3$, 98%, Aldrich); hydrochloric acid (HCl, 37%, Aldrich); sodium hydroxide (NaOH, 97%, Sigma-Aldrich); deuterated perchloric acid ($DClO_4$, 68%, Aldrich).

Crystals of $NaCCl_3SO_3 \cdot H_2O$ and $CsHSO_3$ were prepared as described elsewhere,[41,13] and $CsDSO_3$ was synthesized using D_2O instead of H_2O. Oxygen-free sulfite aqueous solutions for the sulfur XANES absorption and Raman measurements were prepared by dissolving Na_2SO_3 in degassed water to approximately 0.05 and 1 M, respectively, under nitrogen atmosphere. The pH was measured with an IQ150 pH meter equipped with a glass electrode calibrated with standard buffers and adjusted with 1 M HCl or NaOH to pH = 0.0, 3.9 and 10.7 (XANES) and 0.0, 4.1, and 10.8 (Raman), respectively. A 1 M $NaDSO_3$ solution was prepared by dissolving Na_2SO_3 in D_2O and adjusting the pH to 3.9 with concentrated $DClO_4$. Aqueous 0.05 M solutions of $NaCH_3SO_3$, $NaCCl_3SO_3 \cdot H_2O$, and $NaCF_3SO_3$ were obtained by dissolving the salts in water.

Neutron Powder Diffraction. The neutron diffraction pattern of crystalline $CsDSO_3$ powder was collected at the NFL reactor, Studsvik, Sweden, for fixed wavelength (λ = 1.47 Å) at ambient temperature in the 2θ range 4.0−139.9° with $\Delta(2\theta)$ = 0.08°. The Rietveld method implemented in the FULLPROF program was used to obtain the atomic positions.[42] A total of 12 parameters were refined: the overall scale factor; the zero point error for the 2θ angle; two unit cell parameters; three half-width parameters (*U*, *V*, *W*) characterizing the instrumental resolution; one common isotropic displacement (temperature) parameter (B_{iso}) for all atoms; the *z* atomic coordinate for the S and D atoms; the *x* and *z* atomic coordinates for O. Starting parameters were obtained from the single-crystal X-ray diffraction study by Johansson et al.[13] For X-ray diffraction data with high-resolution profiles, it has been proposed that the probable error in Rietveld refinements could be up to 2.93 times the estimated standard deviations due to local correlations.[43] However, as the Rietveld method was developed for neutron data with a classical recording step, the estimated standard deviations reported here are those obtained from the refinements.

The unit cell dimensions were refined from X-ray powder diffraction data recorded with a Guinier-Hägg focusing camera of 40 mm diameter, using monochromatized Cu $K\alpha_1$ radiation (λ = 1.5406 Å). The exposed film was digitized with an LS18 film scanner,[44] background corrected, and evaluated with the SCANPI program.[45] The diffraction pattern was indexed, and the unit cell parameters were refined by means of the PIRUM program with silicon as internal standard.[45]

Vibrational Spectroscopy. Raman spectra of the crystalline compounds cesium sulfonate, its deuterated analogue, sodium methanesulfonate, and sodium trichloromethanesulfonate monohydrate were obtained by means of a Renishaw System 1000 spectrometer, equipped with a Leica DMLM microscope, a 25 mW diode laser (782 nm), and a Peltier-cooled CCD detector. The mid-IR absorption spectra (range 400−4000 cm^{-1}, resolution 4 cm^{-1}) were recorded of the $Cl_3CSO_3Na \cdot H_2O$ and H_3CSO_3Na compounds in KBr pellets and of $CsHSO_3$ and $CsDSO_3$ in Nujol mull using a purged Bio-RAD Digilab FTS 6000 FT-IR spectrometer. Raman spectra of a $NaDSO_3$ solution and of Na_2SO_3 solutions at different

(18) Hendrickson, J. B.; Sternbach, D. D.; Bair, K. W. *Acc. Chem. Res.* **1977**, *10*, 306−312.
(19) Hansen, R. L. *J. Org. Chem.* **1965**, *30*, 4322−4324.
(20) Streitwieser, A., Jr.; Wilkins, C. L.; Keihlmann, E. *J. Am. Chem. Soc.* **1968**, *90*, 1598−1601.
(21) Su, T. M.; Sliwinski, W. F.; Schleyer, P. von R. *J. Am. Chem. Soc.* **1969**, *91*, 5386−5388.
(22) Dueber, T. E.; Stang, P. J.; Pfeifer, W. D.; Summerville, R. H.; Imhoff, M. A.; Schleyer, P. von R.; Hummel, K.; Bocher, S.; Harding, C. E.; Hanack, M. *Angew. Chem., Int. Ed. Engl.* **1970**, *9*, 521−522.
(23) Strauss, S. H. *Chemtracts: Inorg. Chem.* **1994**, *6*, 1−13.
(24) Lawrance, G. A. *Chem. Rev.* **1986**, *86*, 17−33.
(25) Wulfsberg, G.; Cochran, M.; Wilcox, J.; Koritsanszky, T.; Jackson, D. J.; Howard, J. C. *Inorg. Chem.* **2004**, *43*, 2031−2042.
(26) Bürger, H.; Burczyk, K.; Blaschette, A. *Monatsh. Chem.* **1970**, *101*, 102−119.
(27) Miles, M. G.; Doyle, G.; Cooney, R. P.; Tobias, R. S. *Spectrochim. Acta* **1969**, *25A*, 1515−1526.
(28) Varetti, E. L.; Fernandez, E. L.; Ben Altabef, A. *Spectrochim. Acta* **1991**, *47A*, 1767−1774.
(29) Edwards, H. G. M.; Smith, D. N. *J. Mol. Struct.* **1991**, *263*, 11−20.
(30) (a) Gejji, S. P.; Hermansson, K.; Lindgren, J. *J. Phys. Chem.* **1993**, *97*, 3712−3715; (b) Gejji, S. P.; Hermansson, K.; Lindgren, J. *J. Phys. Chem.* **1994**, *98*, 8687−8692.
(31) Thompson, W. K. *Spectrochim. Acta* **1972**, *28A*, 1479−84.
(32) Wei, C. H.; Hingerty, B. E. *Acta Crystallogr.* **1981**, *B37*, 1992−7.
(33) Bolte, M.; Griesinger, C.; Sakhaii, P. *Acta Crystallogr.* **2001**, *E57*, o458−o460.
(34) Jones, P. O.; Kennard, O.; Horn, A. S. *Acta Crystallogr.* **1978**, *B34*, 3125−3127.
(35) Wei, C. H. *Acta Crystallogr.* **1981**, *B37*, 844−849.
(36) Bourne, S. A.; Coetzee, A.; Ndlovu, M. E. *J. Chem. Crystallogr.* **1998**, *28*, 885−892.
(37) Delaplane, R. G.; Lundgren, J. O.; Olovsson, I. *Acta Crystallogr.* **1975**, *B31*, 2202−2207.
(38) Molla-Abbassi, A.; Eriksson, L.; Mink, J.; Persson, I.; Sandström, M.; Skripkin, M.; Ullström, A.-S.; Lindqvist-Reis, P. *J. Chem. Soc., Dalton Trans.* **2002**, *23*, 4357−4364.
(39) Sofina, N.; Peters, E.-M.; Jansen, M. *Z. Anorg. Allg. Chem.* **2003**, *629*, 1431−1436.
(40) Abbasi, A.; Lindqvist-Reis, P.; Eriksson, L.; Sandström, D.; Lidin, S.; Persson, I.; Sandström, M. *Chem.—Eur. J.* **2005**, *11*, 4065−4077.
(41) Damian, E.; Eriksson, L.; Sandström, M. *Acta Crystallogr.* **2006**, *C62*, m419−m420.
(42) Rodriguez-Carvajal, J. FULLPROF: A program for Rietveld Refinement and Pattern Matching Analysis. *Abstracts of the Satellite Meeting on Powder Diffraction of the XV Congress of the IUCr*, Toulouse, France, 1990; p 127. Rodriguez-Carvajal, J., Roisnel, T. FULLPROF98 and WinPLOTR: New Windows 95/NT Application for Diffraction Commission For Powder Diffraction, International Union for Crystallography. *Newslett.* **1998**, *20* (May-Aug), Summer.
(43) (a) Berar, J. F.; Lelann, P. *J. Appl. Crystallogr.* **1991**, *24*, 1−5. (b) Berar, J. F. *NIST Spec. Publ.* **1992**, *846*, 63−67.
(44) Johansson, K. E.; Palm, T.; Werner, P.-E. *J. Phys.* **1980**, *E13*, 1289−1291.
(45) (a) Werner, P.-E.; Eriksson, L.; Salomé, S. *SCANPI, a program for evaluation Guinier photographs*; Stockholm University: Stockholm, 1980. (b) Werner, P.-E. *Ark. Kemi* **1969**, *31*, 513−516.

Table 1. Experimental IR and Raman Fundamental Vibrations (cm^{-1}) with Assignments for the $CsHSO_3$ and $CsDSO_3$ Compounds and Potential Energy Distribution (PED) for the HSO_3^- Ion

$CsHSO_3$		$CsDSO_3$			
IR	Raman	IR	Raman	assgnt	PED (%)
2573 (31)[a]	2573 (30)		2574 (2)[b]	A_1, ν_1, SH stretch	96 ν(SH)
		1871 (40)	1872 (71)	A_1, ν_1, SD stretch	
1196 (96)	1192 (3)	1196 (88)	1190 (5)	E, ν_4, SO_3 asym stretch	56 $\nu_a(SO_3)$, 34 δ(SH)
			1184 sh	E, ν_4, $^{34}SO_3$ asym stretch	
1128 (22)	1122 (87)			E, ν_5, SH bend	62 δ(SH), 30 $\nu_a(SO_3)$
	1110 sh			E, ν_5, ^{34}SH bend	
1037 (56)	1039 (100)	1035 (46)	1036 (100)	A_1, ν_2, SO_3 sym stretch	94 $\nu_s(SO_3)$
1023 vw, sh	1024 vw	1021 sh	1021 (3)	A_1, ν_2, $^{34}SO_3$ sym stretch	
		831 (30)	832 (73)	E, ν_5, SD bend	
629 (76)	627 (4)	625 (61)	632 (4)	E, ν_6, SO_3 asym def	74 $\delta_a(SO_3)$, 18 δ(SH), 8 $\nu_a(SO_3)$
619 sh	619 sh	616 sh		E, ν_6, $^{34}SO_3$ asym def	
507 (100)	515 (27)	500 (100)	504 (23)	A_1, ν_3, SO_3 sym def[c]	96 $\delta_s(SO_3)$
	507 sh	494 sh		A_1, ν_3, $^{34}SO_3$ sym def	

[a] The relative intensities of the bands are given in parentheses after the wavenumbers. For qualitative intensities of the weak bands, the following abbreviations were used: sh, shoulder; vw, very weak; vvw, very very weak; br, broad. [b] Trace of HSO_3^-. [c] Different IR and Raman frequencies due to weak intermolecular interactions in the solid phase.

Table 2. Vibrational Raman Frequencies and Assignments for 1 M Sulfite(IV) Solutions at pH = 0 (SO_2(aq)), pH = 10.8 (SO_3^{2-}), pH = 3.9 ($NaHSO_3$), and pH = 4.1 ($NaDSO_3$)

SO_2(aq)[a]	SO_3^{2-}	$NaHSO_3$	$NaDSO_3$	assgnt[b]
	3407 (10)		2664 (20)	ν(OH) (H_2O)
3375 (21)	3351 (8)	3363 (33)		
3261 (8)	3260 (15)	3264 (12)		
3214 (69)	3212 (100)	3222 (100)	2520 (100)	
		3145 (19)	2385 (40)	ν(OH) [$SO_2(OH)^-$]
		2535 (0.2)	1848 (3)	ν(SH)/ν(SD)
	1659 (7)			overtone 3 × 553
1649 (13)	1632 (50)	1648 (12)	1210 (2)	$\delta(OH_2)/\delta(OD_2)$
1577 (1)				$R(H_2O)$ + 1151
		1545 (2)		1053 + 496
1330 (4)				$\nu_a(SO_2)$
1151 (100)				$\nu_s(SO_2)$
		1210 (0.2)	1210 (0.3)	$\nu_a(SO_3)$ (HSO_3^-)
		1095 (3)	1092 (10)	$\nu_a(SO_2)$ [$SO_2(OH)^-$]
		1126 (5)		δ(SH)
		1082 (38)	937 (13)	ν(SO−H)/ν(SO−D)
		1053 (52)	1052 (37)	$\nu_s(SO_2)$ [$SO_2(OH)^-$]
		1025 (14)	1032 (8)	$\nu_s(SO_3)$ (HSO_3^-)
	1097 (15)			overtone 2 × 553
	967 (85)			$\nu_s(SO_3)$
	934 (23)			$\nu_a(SO_3)$
			925 (80)	$\nu_1(ClO_4^-)$
			836 (0.8)	δ(SD)
	797 (3)			
		648 (4)	657 (2)	$\delta_a(SO_3)$ (HSO_3^-, $S_2O_5^{2-}$)
			632 (8)	$\nu_4(ClO_4^-)$
	613 (19)			
		582 (14)	595 (6)	$\delta(SO_2)$ [$SO_2(OH)^-$]
559 (17)	553 (12)			$\delta(SO_2)/\delta_a(SO_3)$
		496 (17)	505 (14)	$\delta_s(SO_3)$ (HSO_3^-)
	474 (39)			$\delta_s(SO_3)$
			466 (7)	$\nu_2(ClO_4^-)$
		432 (11)	436 (2)	$\tau(SO_2)$ [$SO_2(OH)^-$, $S_2O_5^{2-}$]
		378 (0.6)	384 (0.3)	$\omega(SO_2)$ [$SO_2(OH)^-$]

[a] Relative intensities in parentheses. [b] Notation of vibrational modes: ν, stretching; δ, bending; τ, twisting; ω, wagging; s, symmetric; a, asymmetric.

pH were recorded by means of a dedicated BioRad FT-Raman system equipped with a Spectra Physics Nd:YAG laser (1024 nm, 200 mW). All measurements were performed at ambient temperature. The experimental IR and Raman frequencies for the solid $CsHSO_3$ and $CsDSO_3$ compounds are reported in Table 1, for the sulfite solutions in Table 2, and for $NaCH_3SO_3$ and $NaCCl_3SO_3 \cdot H_2O$ in Table 3, with the corresponding IR and Raman spectra are displayed in Figure 1.

Normal coordinate calculations were performed by means of Wilson's **GF** matrix method. The assignment of the fundamental bands is based on the potential energy distributions and isotopic shifts (Tables 1 and 3), and the refined force constants are summarized in Table 4. A PC-based program package developed by Mink and Mink was used to compute force constants and to fit vibrational frequencies using a symmetrized valence force field.[46]

Geometry optimization followed by vibrational frequency calculations were performed by means of GAUSSIAN98 software at the B3LYP/6-311++G(d, p) level for all the species including the

(46) Mink, J.; Mink, L. M. *Computer Program System for Vibrational Analyses of Polyatomic Molecules (in Lahey-Fujitsu Fortran Win32)*; Stockholm University: Stockholm, 2004; available from J. Mink.

Table 3. Experimental IR and Raman Frequencies of the Normal Modes for the $H_3CSO_3^-$ and $Cl_3CSO_3^-$ Ions (Relative Intensities in Parentheses), with Assignments and Calculated Potential Energy Distribution (PED)

$NaCH_3SO_3$		$NaCCl_3SO_3{\cdot}H_2O$			
IR	Raman	IR	Raman	assgnt	PED[a] (%)
3017 (14)	3017 (45)			E, ν_6, CH_3 asym stretch	$O_3SCH_3^-$, 99 $\nu_a(CH_3)$
2938 (14)	2938 (89)			A_1, ν_1, CH_3 sym stretch	$O_3SCH_3^-$, 99 $\nu_s(CH_3)$
1436 (11) 1417 (15)	1450 (14), 1432 (13), 1413 (13)			E, ν_7, CH_3 asym def[a]	$O_3SCH_3^-$, 95 $\delta_a(CH_3)$, 5 $\rho(CH_3)$
1337 (32)	1337 (3.6)			A_1, ν_2, CH_3 umbrella	$O_3SCH_3^-$, 88 $\delta_s(CX_3)$
1250 (75), 1201 (100)	1214 (5.6), 1201 (10), 1191 (5.8)	1264 (100), 1238 (93)	1256 (10), 1238 (7.8)	E, ν_8, SO_3 asym stretch[a]	$O_3SCH_3^-$, 86 $\nu_a(SO_3)$, 6 $\delta_a(SO_3)$, 5 $\rho(CH_3)$; $O_3SCCl_3^-$, 93 $\nu_a(SO_3)$
1069 (84)	1076 (100), 1060 (15), 1050 (27)	1069 (55)	1076 (30)	A_1, ν_3, SO_3 sym stretch[a]	$O_3SCH_3^-$,65 $\nu_s(SO_3)$, 16 $\delta_s(SO_3)$, 14 ν(CS); $O_3SCCl_3^-$, 90 $\nu_s(SO_3)$, 5 $\delta_s(SO_3)$, 5 ν(CS)
963 (4.8)	982 (3.4), 971 (3.2)			E, ν_9, CH_3 rocking[a]	$O_3SCH_3^-$, 88 $\rho(CH_3)$, 7 $\nu_a(SO_3)$
		814 (34), 802 (71), 791 (44)	828 (11), 805 (16)	E, ν_6, CCl_3 asym stretch[a]	$O_3SCCl_3^-$, 53 $\nu_a(CCl_3)$, 21 $\delta_a(CCl_3)$, 15 $\rho(CCl_3)$, 7 $\rho(SO_3)$
793 (57)	796 (56), 791 (42), 778 (18)	620 (53)	631 (13)	A_1, ν_4, CS stretch[a]	$O_3SCH_3^-$, 43 ν(CS), 33 $\nu_s(SO_3)$, 19 $\delta_s(SO_3)$; $O_3SCCl_3^-$, 34 ν(CS), 34 $\delta_s(CCl_3)$, 30 $\nu_s(CCl_3)$
562 (74)	575 (34), 565 (12), 557 (12)	544 (26)	553 (9.2)	A_1, ν_5, SO_3 umbrella[a]	$O_3SCH_3^-$, 65 $\delta_s(SO_3)$, 32 ν(CS); $O_3SCCl_3^-$, 81 $\delta_s(SO_3)$, 13 ν(CS)
535 (63)	542 (25), 531 (16)	544 (26)	542 (11)	E, ν_{10}, SO_3 asym[a] bending	94 $\delta_a(SO_3)$, 6 $\nu_a(SO_3)$
		415 (26)	415 (100)	A_1, ν_1, CCl_3 sym stretch	$O_3SCCl_3^-$, 41 $\nu_s(CCl_3)$, 36 ν(CS), 21 $\delta_s(CCl_3)$
353 (7.2)	351 (26)	341 (6.3)	341 (37)	E, ν_{11}, SO_3 rocking	$O_3SCH_3^-$, 97 $\rho(SO_3)$; $O_3SCCl_3^-$, 47 $\rho(SO_3)$, 24 $\nu_a(CCl_3)$, 20 $\rho(CCl_3)$
		264 (11)	264 (38)	E, ν_7, CCl_3 asym def	$O_3SCCl_3^-$, 59 $\delta_a(CCl_3)$, 18 $\nu_a(CCl_3)$, 17 $\rho(CCl_3)$
		248 (5)	248 (37)	A_1, ν_2, CCl_3 umbrella	$O_3SCCl_3^-$, 38 $\delta_s(CCl_3)$, 36 ν(CS), 18 $\nu_s(SO_3)$
		185 (6.3)	175 (19)	E, ν_9, CCl_3 rocking	$O_3SCCl_3^-$, 65 $\rho(CCl_3)$, 19 $\rho(SO_3)$, 9 $\nu_a(SO_3)$

[a] Solid-state effects cause splitting of fundamental modes.

hydrated molecules and ions except the sulfite ion (SO_3^{2-}), and the results are reported in Table S-6 (Supporting Information).

X-ray Absorption Spectroscopy. Sulfur K-edge XANES spectra were recorded in fluorescence mode at beamline 6-2 of Stanford Synchrotron Radiation Laboratory (SSRL), operating under dedicated conditions (3 GeV, 75−100 mA). The X-ray energy was varied using a fully tuned liquid-nitrogen-cooled Si(111) double monochromator with the energy scale calibrated by setting the lowest energy peak of sodium thiosulfate ($Na_2S_2O_3{\cdot}5H_2O$) to 2469.2 eV.[47] Higher order harmonics were rejected by means of a nickel-coated mirror. A nitrogen-filled Lytle detector, without filter and Soller slit, was used to detect the fluorescence signal from the sample. The beam path through the monitoring ion chamber and the sample surrounding was in helium of atmospheric pressure. Temperature control of the solutions, enclosed in Teflon spacers between 5 μm polypropylene windows, was achieved combining cooled nitrogen gas flow through a metal block with Peltier heating. For the solid samples, finely ground crystals were dispersed in a thin layer on a sulfur-free Mylar adhesive tape. The data were analyzed using the EXAFSPAK suite of computer programs.[48] Normalized intensity spectra are presented throughout this study.

XANES Computations. The theoretical calculations of XANES spectra were performed by means of the StoBe-deMon DFT program system.[49] The electronic transitions were described by the transition potential (TP) method,[6] using nonlocal exchange and correlation functionals throughout.[50] In short, the orbitals for the molecular species are determined using a high quality molecular basis set with a half-occupied core orbital at the excitation site; i.e., the potential used for the excited states is derived by removing half an electron from the sulfur atom 1s orbital. The transition moments were calculated as the dipole matrix element between the initial and final state using the same set of orbitals to describe both states.[6] The final state relaxation effects, which differ to some extent for each excited state, were computed separately for some of the lowest excited states in a variational treatment by means of the Δ(Kohn−Sham) method.[51]

The description of the central core-excited sulfur atom was extended with a very large, diffuse additional basis set (double basis-set approach).[52] The IGLO-III basis of Kutzelnigg and co-workers was used to describe the relaxation effects of the inner orbitals.[53] Relativistic effects on the S(1s) ionization potential (IP) were calculated for atomic sulfur at the MCPF level (Modified Coupled Pair Functional) using first-order perturbation-theory corrections including the mass−velocity and Darwin terms; this increases the

(47) Sekiyama, H.; Kosugi, N.; Kuroda, H.; Ohta, T. *Bull. Chem. Soc. Jpn.* **1986**, *59*, 575−579.
(48) George, G. N.; Pickering, I. J. *EXAFSPAK; A Suite of Computer Programs for Analysis of X-ray Absorption Spectra*; SSRL, Stanford University: Stanford, CA, 1993.
(49) *StoBe-deMon (Stockholm-Berlin version of deMon, a Density Functional Theory (DFT) molecule/cluster package)*, version 2.1, Mar 2005, StoBe2005; http://w3.rz-berlin.mpg.de/~hermann/StoBe/.
(50) (a) Perdew, J. P.; Wang, Y. *Phys. Rev. B* **1986**, *33*, 8800−8802. (b) Perdew, J. P. *Phys. Rev. B* **1986**, *33*, 8822−8824. (c) Perdew, J. P. *Phys. Rev. B* **1986**, *34*, 7406.
(51) Kolczewski, C.; Püttner, R.; Plashkevych, O.; Ågren, H.; Staemmler, V.; Martins, M.; Snell, G.; Schlachter, A. S.; Sant'Anna, M.; Kaindl, G.; Pettersson, L. G. M. *J. Chem. Phys.* **2001**, *115*, 6426−6437.
(52) Ågren, H.; Carravetta, V.; Vahtras, O.; Pettersson, L. G. M. *Theor. Chem. Acc.* **1997**, *97*, 14−40.
(53) Kutzelnigg, W.; Fleischer, U.; Schindler, M. *NMR-Basic Principles and Progress*; Springer-Verlag: Heidelberg, Germany, 1990.

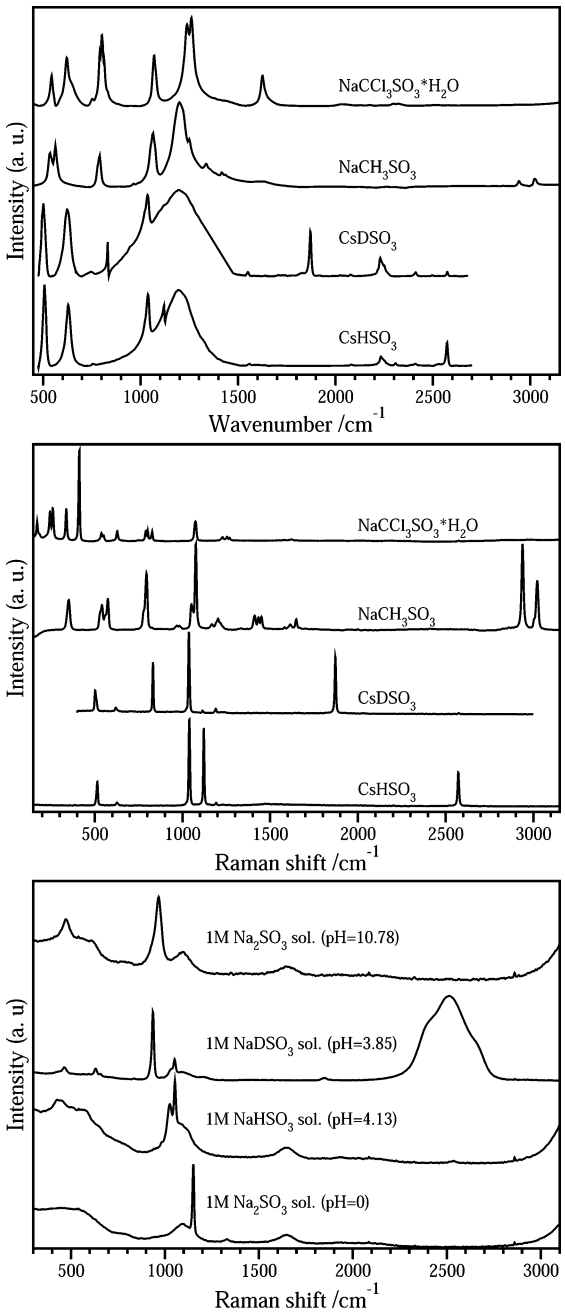

Figure 1. Experimental IR (top) and Raman (middle) spectra of the solid compounds $Cl_3CSO_3Na\cdot H_2O$, H_3CSO_3Na, $CsHSO_3$, and $CsDSO_3$ and (bottom) the Raman spectra of sodium sulfite in aqueous solution at pH = 0, 4.1, and 10.8 and of $NaDSO_3$ at pH = 3.9.

calculated S(1s) IP by 7.4 eV. This atomic correction was applied as an overall shift of the energy scale of each spectrum. The absolute energies obtained in this way have been shown in previous computational studies to provide satisfactory agreement for neutral molecules.[51,54] However, other experimental calibration schemes are also in use for the sulfur K-edge,[3c] e.g., with the peak energy of the first main thiosulfate spectral feature set to 2472.02 eV, i.e., +2.82 eV higher energy than the present scale.[55]

The corrected excitation energies and their corresponding transition moments were used to generate a theoretical spectrum by convoluting the discrete spectral transitions with a Gaussian function. A certain full width at half-maximum (FWHM) was chosen to match the experimental bandwidth for the region below the ionization potential (IP). That includes the instrumental broadening of the spectral features, which is ca. 0.5 eV,[3] and also broadening due to hydrogen bonding and symmetry breaking vibrational and surrounding effects. The FWHM of the Gaussian was linearly increased to 8 eV for the next 20 eV and then kept constant at 8 eV to simulate the approach toward continuum at higher energies and ascertain that no spurious, basis-set dependent resonances are displayed in the continuum. The calculated XANES features, with transition energies and moments modified in this way, could then be directly compared with the experimental XANES spectrum. Note that either by adding the augmentation basis also to surrounding centers or by sampling various slightly modified structures to simulate environmental effects on the solvated species, the discrete representation of the continuum can be made denser allowing a smaller FWHM of the broadening function to be applied.

The following orbital basis sets were employed during the calculations: the TZVP ((6311/311/1)) set for oxygen; (311/1) for hydrogen; DZVP (6321/521/1*) for chlorine; DZVP3 (6311/311/1) for carbon and fluorine. Auxiliary basis sets were introduced: (5,4;5,4) for sulfur and chlorine; (5,3;5,3) for oxygen and carbon; (5,2;5,2) for fluorine; (4,2;4,2) for hydrogen. The nomenclature ((N_C(s), N_C(spd); N_{XC}(s), N_{XC}(spd)) indicates the number of s- and spd-type functions that were used to fit and expand the Coulomb and exchange-correlation potentials, respectively. The Cs^+ ion in the $CsHSO_3$ solid was described using the pseudopotential description by Leininger et al.[56] in the representation proposed by Pelissier and co-workers.[57]

Sulfur atoms other than the core-excited one were described by means of an effective core potential with a [5s,4p,1d] basis set contracted as (311/211/1) to eliminate the S(1s,2s,2p) levels, using a procedure described elsewhere.[58]

Results and Discussion

Neutron Diffraction of $CsDSO_3$. The compound crystallizes in space group *R*3*m* (No. 160) with the unit cell dimensions (hexagonal setting) $a = b = 6.326(1)$ Å, $c = 8.718(1)$ Å, $\alpha = \beta = 90°$, $\gamma = 120°$, and $Z = 3$. The refined atomic coordinates are listed in Table S-1, and the observed and calculated neutron diffraction patterns are displayed in Figure S-1. The bond distances obtained, S−O 1.44(1) Å and S−D 1.38(2) Å, were used in the models for normal coordinate analyses and XANES computations. Nine oxygen atoms surround the Cs^+ ion, with three Cs···O contact distances of 3.20(2) Å and six of 3.25(1) Å.

Vibrational Analyses of Sulfite(IV) Species. The remeasured vibrational spectra of the $CsHSO_3$ and $CsDSO_3$ compounds (Figure 1) were analyzed by means of normal coordinate methods. The 9 fundamental vibrations of the sulfonate ion belong to two types of symmetry species, $3A_1 + 3E$ in the C_{3v} point group, resulting in six IR- and Raman-

(54) Odelius, M.; Cavalleri, M.; Nilsson, A.; Pettersson, L. G. M. *Phys. Rev. B* **2006**, *73*, 024205/1−024205/6.
(55) Rompel, A.; Cinco, R. M.; Latimer, M. J.; McDermott, A. E.; Guiles, R. D.; Quintanilha, A.; Krauss, R. M.; Sauer, K.; Yachandra, V. K.; Klein, M. P. *Proc. Natl. Acad. Sci. U.S.A.* **1998**, *95*, 6122−6127.
(56) Leininger, T.; Nicklass, A.; Küchle, W.; Stoll, H.; Dolg, M.; Bergner, A. *Chem. Phys. Lett.* **1996**, *255*, 274−280.
(57) Pelissier, M.; Komiha, N.; Daudey, J. P. *J. Comput. Chem.* **1988**, *9*, 298−302.
(58) Pettersson, L. G. M.; Wahlgren, U.; Gropen, O. *J. Chem. Phys.* **1987**, *86*, 2176−2184.

Table 4. Calculated Force Constants for Oxosulfur Species

internal coordinates		SO_2[d]	SO_2(aq)[e]	SO_3^{2-}[f]	SO_4^{2-}[g]	SO_3[h]	HSO_3^-[i]	$O_3SCH_3^-$[j]	$O_3SCCl_3^-$[k]	$O_3SCF_3^-$[l]
stretch[a]	*K*(SO)	10.065	9.896	5.366	6.592	10.24	7.956	7.601	8.516	8.346
	K(CS/HS/SS)						3.800	3.967	2.573	3.492
	K(CX); X = H, Cl, F							4.881	2.847	5.758
stretch−stretch[a]	*f*(SO, SO)	0.059	0.040	0.690	0.857	0.22	0.164	0.044	0.056	−0.266
	f(CX, CX)							0.109	0.469	2.607
bending[b]	*H*(OSO)	1.626	1.780	2.295	2.638	1.321	2.571	1.923	1.804	2.082
	H(OSH/OSC/OSS)						0.695	1.016	1.060	1.230
	H(XCS)							0.666	1.498	0.691
	H(XCX)							0.629	1.601	1.984
	H(SO_3 out-of-plane bending)					0.632				
bending−bending[b]	*h*(OSO, OSO)			0.620	0.603			0.362	0.060	
	h(XCS, XCS)							−0.078		0.223
	h(XCX, XCX)							0.044	0.034	
	h(OSC, OSC/OSH, OSH/OSS, OSS)						−0.311	0.495		0.796
stretch−bend[c]	*k*(SO, OSO)	0.374	0.441							
	k(CX, XCX)								0.710	0.460
	k(CS, XCS)								1.210	−0.387
S−O bond (Å)		1.432	1.469	1.505	1.472	1.43	1.441	1.454	1.448	1.433

Force constant units: [a] 10^2 N·m^{-1}; [b] 10^{-18} N·m·rad^{-2}; [c] 10^{-8} N·m·rad^{-1}. [d] References 67, 74 (geometry), 67 and 75 (frequencies and force constants). [e] S−O bond length from Gaussian geometry optimization, this work; ref 60 (frequencies). [f] References 66 (geometry), 76, 77 (frequencies and force constants). [g] References 65 (geometry), 78, 79 (frequencies). [h] References 74 (geometry), 80, 81 (IR and Raman frequencies). [i] References 15, 17 (frequencies), geometry this work. [j] References 33 (geometry), 31 (frequencies). [k] References 41 (geometry), 26, 27, 29 (frequencies and force constants). [l] References 39 (geometry), 38, 27, 30 (frequencies and force constants). Solid-state geometry is used except for SO_2(g) and SO_3(g).

active vibrational modes. All show strong IR activity, but in the Raman spectra the symmetric deformation (umbrella mode, ν_3) and the asymmetric stretching (ν_4) modes of the SO_3 group are weak (Table 1, Figure 1). The largest frequency shift due to deuteration occurs as expected for the SH/SD stretching (ν_1) modes, from 2573 to 1872 cm^{-1}, respectively. The ratio (1.374) is very close to that (1.375) between the stretching frequencies, 2591 and 1885 cm^{-1}, of the HS and DS radicals, respectively.[59] This indicates very weak coupling of the SH/SD stretching with the symmetric SO stretching and SO_3 umbrella modes, consistent with the potential energy distribution (PED in Table 1) for the ν_1 symmetric stretching.

The intense Raman feature at 1039 cm^{-1} (1036 cm^{-1} for $CsDSO_3$) was assigned as the symmetric SO_3 stretching mode (ν_2), and the bands at 1196 cm^{-1} with high IR intensity were assigned as the asymmetric SO_3 stretch (ν_4). The asymmetric SO_3 deformation (ν_6) and the symmetric SO_3 deformation (ν_3, umbrella) modes were assigned as the 629 and 515 cm^{-1} IR and Raman bands, respectively (Table 1). Deuteration shifted ν_6 by about 4−5 cm^{-1} and ν_3 by about 7−11 cm^{-1}, while ν_2 and ν_4 were almost unaffected. A distinct lattice mode occurs as a low-frequency Raman band at 134 cm^{-1}.

Weak features appeared on the low-frequency side of some strong fundamental bands. Such Raman bands at 1110, 1024, 619, and 507 cm^{-1} for HSO_3^- were assigned as the ν_5, ν_2, ν_6, and ν_3 fundamentals of the $H^{34}SO_3^-$ isotopomer. Similar weak bands at 1021, 616, and 494 cm^{-1} were found for the $D^{34}SO_3^-$ ion. The calculated frequencies for the $H^{34}SO_3^-$ and $D^{34}SO_3^-$ ions (Table S-2) support the assignments presented in Table 1. Other weak features in the vibrational spectra could be assigned as overtones and binary combination bands (Table S-3).

Raman spectra of 1 M sodium sulfite solutions at pH = 0 (in 1 M HCl) and at pH = 10.8 (NaOH added), and also of 1 M $NaHSO_3$ and $NaDSO_3$ solutions at about pH = 4−5 (Figure 1), prepared by adding HCl and $DClO_4$, respectively, have been used to identify characteristic bands for the different sulfur(IV) species in aqueous solutions. The experimental frequencies are listed together with the proposed assignments in Table 2.

The strong bands at 3145/2385 cm^{-1} in the $NaHSO_3$/$NaDSO_3$ solutions, respectively, were assigned as the OH/OD stretching modes of the hydrogen sulfite ions, while the weak bands at 2535/1848 cm^{-1} are close to the SH/SD stretching modes in solid cesium sulfonate, respectively, and are assigned as such. For the DSO_3^- ion the asymmetric bending mode is assigned as the weak band at 657 cm^{-1}. It has a slightly "negative" isotope effect! The SO stretching vibrations of different S(IV) species are found in the region 934−1330 cm^{-1}. The highest frequencies are expected for the hydrated sulfur dioxide molecule with strong S−O bonding, and the Raman bands at 1330 and 1151 cm^{-1} are assigned as SO_2 asymmetric stretching and symmetric stretching, respectively, in agreement with previous studies.[60,61] The corresponding symmetric and asymmetric stretching Raman bands for the sulfite ion SO_3^{2-} in Na_2SO_3 solution are at 967 and 934 cm^{-1}, respectively. In this case the symmetric SO stretch is higher than the asymmetric.

Several bands were observed in the regions 1025−1210 cm^{-1} for $NaHSO_3$(aq) and 836−1210 cm^{-1} for $NaDSO_3$(aq), which contain both hydrogen sulfite and sulfonate ions, Table 2, and have been assigned by analyzing their relative intensities and isotopic shifts. The medium intensity band at 1126/836 cm^{-1} with the largest shift at

(59) Acquista, N.; Schoen, L. J. *J. Chem. Phys.* **1970**, *53*, 1290−1291.

(60) Zhang, Z.; Ewing, G. E. *Spectrochim. Acta* **2002**, *A58*, 2105−2113.

(61) Davis, A. R.; Chatterjee, R. M. *J. Solution Chem.* **1975**, *4*, 399−412.

deuteration was assigned as the SH/SD bending mode of the sulfonate ion, and the strong band at 1082/937 cm^{-1}, as the S−O(H/D) stretch of hydrogen sulfite. Among the less shifted spectral features the weak band at 1210 cm^{-1} was assigned as the asymmetric SO_3 stretching of the sulfonate ion, and the medium intensity band at 1095/1092 cm^{-1}, to the asymmetric SO_2 stretch of hydrogen sulfite. The corresponding symmetric stretching modes occurred at somewhat lower frequencies. The strong bands at 1053/1052 cm^{-1} were assigned as the SO_2 symmetric stretching mode of the hydrogen sulfite (SO_3H^-/SO_3D^-) ions, and the medium intensity bands at 1025/1032 cm^{-1}, as the SO_3 symmetric stretch of the sulfonate (HSO_3^-/DSO_3^-) ions. In 1 M sulfite solution around this pH value up to about 0.2 M disulfite ions ($S_2O_5^{2-}$) could be expected according to UV data,[62] with Raman bands at 430, 665, and 1050 cm^{-1},[11,12,16] partially overlapped by other stronger modes (Table 2). However, the weakness of the bands around 430 and 650 cm^{-1} indicates the disulfite amount to be rather small.

The assignment of the bending modes was less straightforward. For the sulfite (SO_3^{2-}) solution, the strong Raman band at 474 cm^{-1} was assigned as the SO_3 umbrella mode and the medium intensity band at 553 cm^{-1} as the asymmetric deformation mode. For the hydrogen sulfite ion (SO_3H^-/SO_3D^-) three bands are expected for the scissoring, twisting, and wagging modes and two bands for the sulfonate (HSO_3^-/DSO_3^-) umbrella and rocking modes. Comparisons with sulfonate in the solid state allowed the following assignments: the medium intensity bands at 496/505 cm^{-1} as the sulfonate umbrella mode and the bands at 648/657 cm^{-1} as sulfonate asymmetric deformation. For hydrogen sulfite the tentative assignments were as follows: scissoring at 582/595 cm^{-1}, twisting at 432/436 cm^{-1}, and wagging at 378/384 cm^{-1}, with the rocking mode expected at a lower frequency.

Vibrational Analysis of the Substituted Sulfonates $X_3CSO_3^-$, X = H, Cl, and F. The Raman and IR spectra of sodium methanesulfonate and trichloromethanesulfonate were measured (Figure 1) and compared with our previous study of trifluoromethanesulfonate.[38] Distortions of the $X_3CSO_3^-$ ions from C_{3v} symmetry or coupling of the oscillators in the solid state will split or shift degenerate vibrational modes. Splittings were observed especially in the Raman spectra of sodium methanesulfonate and complicated the assignment of the normal modes (Table 3). In both the Raman and IR spectra two bands were observed near 3000 cm^{-1}. On the basis of their relative intensities, we assigned the strong Raman band at 2938 cm^{-1} as symmetric (A_1) and the band at 3017 cm^{-1} as asymmetric (E) C−H stretching. Methyl group deformations are usually observed in the range 1300−1500 cm^{-1}; thus the set of Raman bands at 1450, 1432, and 1413 cm^{-1} and the IR bands at 1436 and 1417 cm^{-1} were assigned as asymmetric bendings, and the band at 1337 cm^{-1} was assigned as symmetric deformation. Methyl group rocking appeared as weak IR bands at 982 and 971 cm^{-1} in Raman and 963 cm^{-1} in IR. The strongest Raman band at 1076 cm^{-1} was, together with its satellites at 1060 and 1050 cm^{-1}, attributed to SO symmetric stretching, and the strongest IR band at 1201 cm^{-1} (with a satellite at 1250 cm^{-1}), to SO asymmetric stretching. The set of strong Raman bands at 796, 791, and 778 cm^{-1} (793 cm^{-1} in IR) was assigned as CS stretches, the sets of Raman bands at 575, 565, and 557 cm^{-1} and 542 and 531 cm^{-1} (562 and 535 cm^{-1} in IR) were assigned as SO_3 symmetric and asymmetric bending modes, respectively, and the Raman band at 351 (IR 353) cm^{-1} was assigned as the SO_3 rocking mode. Table S-4 lists all observed bands, including combination bands and overtones.

Replacement of the methyl groups leads to substantial changes in the high-frequency region of the spectra; e.g., for trichloromethanesulfonate all vibrational frequencies shift down significantly: the symmetric C−Cl stretch to 415 cm^{-1}; asymmetric stretches to 814, 802, and 791 cm^{-1} (IR)/828 and 805 cm^{-1} (Raman); C−Cl bending modes to 248 cm^{-1} (symmetric) and 264 cm^{-1} (asymmetric); rocking to 185 (IR)/175 cm^{-1} (Raman).

For the $X_3CSO_3^-$ anions the C−S stretching modes obtain the frequencies 793, 620, and 320 cm^{-1} for X = H, Cl, and F, respectively, due to the increasing mass but also due to the change in the C−S bonding and the coupling with other modes (Table 3). The SO_3 group vibrations are far less affected, and the SO stretching modes were observed in the range 1038−1285 cm^{-1} with the largest separation for the trifluoromethanesulfonate ion,[38] the SO_3 bendings at 512−637 cm^{-1}, and the rocking modes at 341−353 cm^{-1}. The assignments, which are based on force field analysis of the averaged frequencies (Table S-5), agree fairly well with those proposed by Miles et al.[27] and Gejji et al.[30] but differ somewhat from those in ref 26.

Force Field Analysis. A symmetrized force field was used for which a consistent set of force constants was refined by fitting the calculated frequencies to the experimental, which were averaged when split. The experimental and the calculated vibrational frequencies for the normal modes of some oxosulfur species are given in Tables S-2, S-5, and S-7, with the refined internal valence force constants summarized in Table 4.

The SH stretching force constant for the sulfonate (HSO_3^-) ion in $CsHSO_3$ is 3.80 N cm^{-1}, which is close to the value for diatomic HS, 3.89 N cm^{-1}. The anharmonicity of the SH and SD stretching (ν_1) and bending modes (ν_5) causes some deviations between experimental and calculated frequencies, while for the other modes the agreement is satisfactory. The localized nature of the SH stretching mode is evident with 96% contribution in the PED and without significant interactions with other totally symmetric modes, Table 1. The SH stretching and bending frequencies of $RbHSO_3$,[15] at 2616 and 1135 cm^{-1}, respectively, are slightly higher than those for $CsHSO_3$, resulting in a higher SH stretching force constant (3.91 N cm^{-1}). The decrease to 2535 cm^{-1} in aqueous solution (Table 2) indicates a weakened SH bond.

For the $X_3CSO_3^-$ ions, X = H, Cl, and F, the evaluation of the stretching force constants for the bonds to the central sulfur atom allows a comparison of the bond character where

(62) Connick, R. E.; Tam, T. M.; von Deuster, E. *Inorg. Chem.* **1982**, *21*, 103−107.

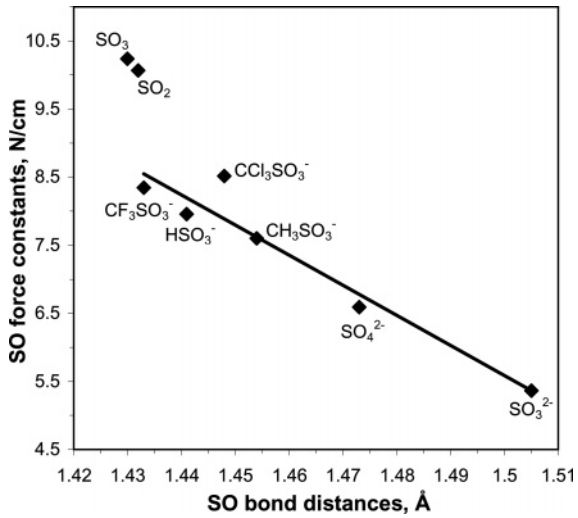

Figure 2. Correlation between S−O stretching force constants and SO bond distances (cf. Table 4) in oxosulfur species.

the mass dependence and the coupling with other modes is eliminated (cf. the PED in Table 3). The CS stretching force constant for methanesulfonate $H_3C-SO_3^-$, 3.97 N cm^{-1}, is slightly higher than for the $H-SO_3^-$ bond in the sulfonate ion. The highly electronegative CF_3 group of trifluoromethanesulfonate, $F_3C-SO_3^-$,[63] lowers the CS force constant somewhat to 3.49 N cm^{-1}. For trichloromethanesulfonate, $Cl_3C-SO_3^-$, the much lower value, 2.57 N cm^{-1}, must largely be an effect of the steric repulsion between the CCl_3 and SO_3 groups. Examination of the intramolecular distances in the trichloromethanesulfonate ion shows that the six closest Cl···O distances in the staggered conformation range from 3.11 to 3.25 Å,[41] mean value 3.18 Å, which is slightly less than the sum of the nonbonded van der Waals radii, 1.81 Å (Cl) + 1.40 Å (O).[64]

The S−O stretching force constants have also been evaluated for some oxosulfur anions and for sulfur dioxide and sulfur trioxide (Table 4) and plotted vs the mean S−O bond length in Figure 2. As could be expected, the S−O stretching force constants generally decrease with increasing mean S−O bond distance except for one clear exception, the trichloromethanesulfonate ($Cl_3CSO_3^-$) ion. The mean O−S−O bond angle (within parentheses) in the pyramidal SO_3 group decreases in the order $Cl_3C-SO_3^-$ (114.2°),[41] $F_3C-SO_3^-$ (113.8°),[39] $H_3C-SO_3^-$ (113.6°),[33] $H-SO_3^-$ (113.1°),[13] $O-SO_3^{2-}$ (109.47°),[65] and SO_3^{2-} (105.7°).[66] Generally, the bond angle increases with increasing S−O force constant, even though steric effects of the group in the fourth (tetrahedral) bonding position evidently have influence. In particular the lone electron pair of the sulfite ion, $:SO_3^{2-}$, increases the S−O bond lengths and decreases the bond angle (Figure 2). Conversely, the planar sulfur trioxide (O−S−O 120°) and the sulfur dioxide molecules (119.53° in the gas phase)[67] with large bond angles have high S−O stretching force constants.

For the sulfonate ion the SO stretching force constant is higher than for methanesulfonate (Table 4). The methyl group is slightly more electronegative ($\chi_G = 2.31$, Pauling scale)[68] than the hydrogen atom ($\chi_G = 2.20$) yet considered a better donor than is the hydrogen atom.[63] The Mulliken population analysis shows a noteworthy charge transfer from the methyl carbon atom to sulfur (Table 5). The sulfur atom s electron population is much higher for the hydrated methanesulfonate ion compared to sulfonate, while other electron populations for the sulfur and oxygen atoms do not differ much.

When a comparison is made of methanesulfonate with trifluoromethanesulfonate, the most significant effect on the electron population from the strongly electronegative CF_3 group ($\chi_G = 3.47$)[63] is the reduction in s and especially in p electron density at the carbon atom and also the slightly lower p electron population at the sulfur atom. The trichloromethanesulfonate ion shows the lowest population of oxygen p electrons, consistent with high π-back-bonding to sulfur. The S−O force constant is also higher than that for the sulfonate and trifluoromethanesulfonate ions, even though the mean S−O bond length in the SO_3 group is longer (Table 4). Despite the high electronegativity of the CCl_3 group ($\chi_G = 2.95$), the carbon s and p populations are much higher than for trifluoromethanesulfonate and almost as high as for methanesulfonate (Table 5). Especially the reduced overlap of the s orbitals, which have the greater electron-attracting power,[63] would reduce the expected electronegativity effect of the CCl_3 group. The result is that the trichloromethanesulfonate ion has the longest CS bond with the lowest C−S stretching force constant of the $X_3CSO_3^-$ ions, X = H, Cl, or F, and also the highest S−O force constant without significant reduction of the mean S−O bond distance.

A useful correlation for force field analyses can be obtained between the frequency separation $\Delta\nu$ of the antisymmetric and symmetric SO_3 stretching modes and the stretch−stretch, f(SO, SO), interaction force constant (Table 4). The plot in Figure S-2 can approximately be described with a linear correlation:

$$f(\mathrm{SO, SO}) = -0.0033(\Delta\nu) + 0.5928 \qquad (1)$$

Generally, with increasing S−O stretching force constants, the O−S−O bond angles increase and the stretch−stretch interaction terms decrease (Table 5), which leads to an increasing frequency separation, again with one exception, the $Cl_3CSO_3^-$ ion.

Figure S-2 and eq 1 show that when the symmetric and antisymmetric SO_3 stretching frequencies are equal, i.e., the

(63) Huheey, J. E.; Keiter, E. A.; Keiter, R. L. *Inorganic Chemistry-Principles of Structure and Reactivity*, 4th ed.; HarperCollins College Publishers: New York, 1993; p 197.
(64) Emsley, J. *The elements*, 3rd ed.; Clarendon Press: Cambridge, U.K., 1998.
(65) Rasmussen, S. E.; Jorgensen, J.-E.; Lundtoft, B. *J. Appl. Crystallogr.* **1996**, *29*, 42−47.
(66) Larsson, L. O.; Kierkegaard, P. *Acta Chem. Scand.* **1969**, *23*, 2253−2260.
(67) Shelton, R. D.; Nielsen, A. H.; Fletcher, W. H. *J. Chem. Phys.* **1953**, *21*, 2178−2183.
(68) Bratsch, S. G. *J. Chem. Educ.* **1988**, *65*, 223−227.
(69) Stumm, W.; Morgan, J. J. *Aquatic chemistry-Chemical equilibria and rates in natural waters*, 3rd ed.; John Wiley & Sons, Inc.: New York, 1996; p 225.
(70) Woronowicz, E. A.; Robertson, W. H.; Weddle, G. H.; Johnson, M. A.; Myshakin, E. M.; Jordan, K. D. *J. Phys. Chem. A* **2002**, *106*, 7086−7089.

Table 5. Mulliken Ground-State Population Analyses for Sulfur Dioxide, the Hydrated Sulfite (SO_3^{2-}), Sulfonate (HSO_3^-), and the Substituted Sulfonate Ions, $X_3CSO_3^-$, X = H, Cl, and F

	SO_2				$SO_3^{2-} + 21H_2O$				$HSO_3^- + 3H_2O$				$CH_3SO_3^- + 3H_2O$				$CCl_3SO_3^- + 3H_2O$				$CF_3SO_3^- + 3H_2O$			
atom	s	p	d	charge	s	p	d	charge	s	p	d	charge	s	p	d	charge	s	p	d	charge	s	p	d	charge
S	5.65	8.66	0.59	1.10	6.43	8.90	0.74	−0.07	5.18	8.58	1.09	1.15	4.46	8.55	1.11	1.88	4.64	8.40	1.13	1.83	4.51	8.31	1.17	2.01
O_1-O_3	4.08	4.44	0.03	−0.55	3.71	4.80	0.02	−0.53	3.88	4.80	0.03	−0.71	3.94	4.91	0.03	−0.88	4.02	4.74	0.03	−0.79	3.99	4.92	0.03	−0.94
C													3.54	3.20	0.03	−0.77	3.41	3.03	0.08	−0.52	2.90	2.14	0.18	0.78
X_1-X_3									1.02	0.01	0.00	−0.03	0.81	0.01	0.00	0.18	5.94	10.99	0.03	0.04	4.01	5.31	0.02	−0.33

frequency separation $\Delta\nu = 0$, then *f*(SO, SO) is close to 0.60 N cm^{-1} and when the band separation is around 180 cm^{-1}, the *f*(SO, SO) interaction term would become close to zero. Figures 2 and S-2 have some practical importance, namely for predicting the SO stretching force constant from the S−O bond distance and the SO−SO interaction force constant from the experimental band separations, respectively, to build up a reliable starting force field for normal coordinate analyses.

Sulfur K-Edge XANES Spectroscopy. Sulfur Dioxide. Sulfur K-edge XANES spectra of SO_2(g), SO_2 dissolved in the non-hydrogen-bonding solvent acetonitrile, SO_2(aq) in aqueous solution with pH = 1.1, and an aqueous solution of 0.05 M Na_2SO_3 at pH = 0 (1 M HCl) show similar preedge features (Figure 3), clearly indicating that the SO_2 molecule is the dominating species. However, in the acidic aqueous solutions the two features between 2475.5 and 2478 eV have merged into a broad band. The spectrum obtained for SO_2(g) dissolved in water at pH ≈ 1.1 (Figure 3d) shows, beside the XANES features of SO_2(aq), a minor contribution at about 2475 eV from the main bands in the spectrum of the Na_2SO_3 solution at pH = 3.9, which contains a mixture of the hydrogen sulfite and sulfonate ions (Figure 3b), consistent with the fractions of sulfite species expected from the diagram calculated for the pH dependence of the sulfite system (Figure 3).[69]

The gas-phase geometry (C_{2v} symmetry, Table 6) of SO_2(g) from a microwave study[67] was used to calculate the electronic S(1s) transitions and generate a XANES spectrum as described above (Figure 3g). Separate relaxation effects for the 11 first states ($5A_1$, $3B_1$, and $3B_2$) were computed and applied: 1, −3.67 eV; 2 and 3, −3.74 eV; 4, −4.19 eV; 5, −4.31 eV; 6, −4.35 eV; 7, −4.73 eV; 8, −4.18 eV; 9, −4.04 eV; 10, −3.68 eV; 11, −4.10 eV. For the remaining states their average value (−4.07 eV) was used, together with the relativistic correction (+7.4 eV).

The main features in the XANES spectrum calculated for the SO_2 molecule (Figure 3g) correspond in order of increasing energy to (1) transition to the totally antibonding π_g* lowest unoccupied molecular orbital (LUMO) belonging to the symmetry species B_1, (2) LUMO+1 (A_1) characterized by in-plane π* mixing between oxygen $2p_x$ and $2p_z$ atomic orbitals, (3) LUMO+2 (B_2), representing the other oxygen $2p_x$ and $2p_z$ orbital combination, and (4) LUMO+4 (B_1), which is a Rydberg dominated state with little valence character. The LUMO+3 (A_1) is dominated by s-character with little p admixture (Figure S-3), and the corresponding electronic transition is not observed in the experimental spectrum.

The agreement between the calculated absolute transition energies and the experimental spectrum with the current energy calibration scheme is quite satisfactory (within 0.2 eV) for the uncharged SO_2 molecule in all aggregation states. When increasing the S−O bond distance 0.03 Å from the microwave value 1.432 Å,[67] the calculated transition energy

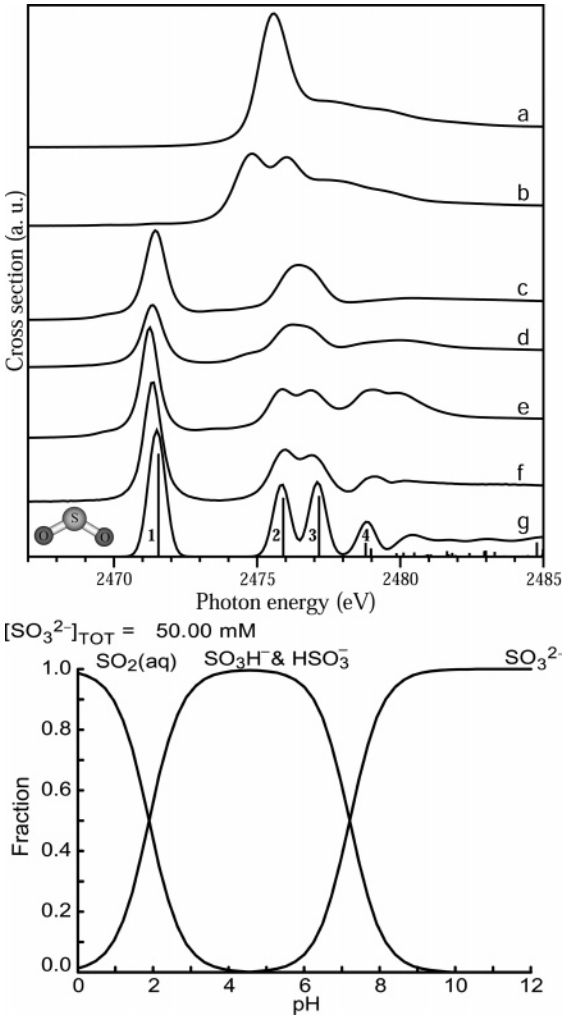

Figure 3. Top: Sulfur K-edge XANES spectra. Key: (a) Na_2SO_3(aq) at pH = 10.7; (b) Na_2SO_3(aq) at pH = 3.9; (c) Na_2SO_3(aq) at pH = 0; (d) SO_2(aq) (ca. 5% in water, pH = 1.1; note the contribution of a minor amount of SO_3H^-); (e) SO_2 dissolved in CH_3CN; (f) SO_2(g); (g) theoretical SO_2 spectrum (S−O 1.432 Å, OSO 119.53°) obtained by convoluting calculated absorption energies and cross sections (vertical bars) with Gaussian functions with FWHM of 0.7 eV below the ionization threshold IP = 2477.4 eV, linearly increased to 8 eV up to about 2497.4 eV. Bottom: Fraction diagram showing the major species expected in 0.05 M sulfite(IV) solution at different pH values with equilibrium constants from ref 69.

(71) Loerting, T.; Liedl, K. R. *J. Phys. Chem. A* **2001**, *105*, 5137−5145.

Table 6. Interatomic Distances (Å) and Angles (deg) Used in the Computation of XANES Spectra for the Sulfur Dioxide Molecule[67] and the Hydrated Sulfonate, Hydrogen Sulfite, Sulfite, Methanesulfonate, Trichloromethanesulfonate, and Trifluoromethanesulfonate Ions

param	SO_2(g)	SO_3H^-	HSO_3^-	SO_3^{2-}	$CH_3SO_3^-$	$CCl_3SO_3^-$	$CF_3SO_3^-$
O_1-S	1.432	1.512	1.441	1.505	1.454	1.448	1.433
O_2-S	1.432	1.502	1.441	1.505	1.454	1.448	1.433
O_3-S		1.60	1.441	1.505	1.454	1.448	1.433
H_I-S, O_3-H_I		0.969	1.381				
$C-S$					1.762	1.847	1.809
X^a-C					1.098	1.766	1.310
O_1-S-O_2	119.53	112.1	115.3	105.7	113.6	114.2	113.8
O_1-S-O_3		99.9	115.3	105.7	113.6	114.2	113.8
O_2-S-O_3		103.6	115.3	105.7	113.6	114.2	113.8
X^a-C-X^a					109.5	109.9	108.7
$O_{1-3}-S-C$					104.9	104.2	104.7
$O_{1-3}-S-H_I$			102.8				
$S-O_3-H_I$		102.1					
$H_W-O_W-H_W{}^b$		105.0	105.0	105.0	105.0	105.0	105.0
H_W-O_W		0.95	0.95	0.95	0.95	0.80[c]	0.95
$H_W-O_I{}^b$		1.80	1.80	1.80	1.80	2.14[c]	1.80

[a] X = H, Cl, or F in $X_3CSO_3^-$. [b] W = water; I = isomer. [c] From the crystal structure.[41]

increases 0.13 eV for the LUMO, while the LUMO+1 and LUMO+2 energies decrease 0.26 eV. However, our calculations also showed that the energy separation between the antibonding combination of oxygen $2p_x$ and $2p_z$ orbitals in the LUMO+1 and LUMO+2 transitions (2 and 3, Figure 3**)** is quite sensitive to the OSO angle (Figure S-4). At OSO 110°, close to the tetrahedral angle, those transitions obtained the same energy. The acetonitrile solution spectrum fits well to a calculated angle of about 119°, similar to the gas-phase value, while an OSO angle of about 115.5−116° was found to satisfactorily reproduce the experimental energy separation for LUMO+1 and LUMO+2 in aqueous solution (Figure 4). Evidently, the hydrogen bonding in aqueous solution affects the geometry of the SO_2 molecule and decreases the OSO angle with about 3°. Such an effect is also indicated when comparing the vibrational frequencies of SO_2(g) and SO_2(aq). The symmetric stretch ν_1, 1151.38 and 1151 cm^{-1}, does not change while the asymmetric ν_3 mode is reduced from 1361.76 to 1332 cm^{-1}, and the bending ν_2 mode increases from 517.69 to 527 cm^{-1}, respectively.[60,61] We performed geometry optimizations and frequency calculations in GAUSSIAN98 (B3LYP/6-311++G(d, p)) for an SO_2 molecule (S−O 1.458 Å, OSO 118.7°) and obtained the frequencies 1131.1 (ν_1), 1309.8 (ν_3), and 504.0 (ν_2) cm^{-1}). For a symmetrical (C_{2v}) chelating hydrogen-bonded $SO_2 \cdot H_2O$ complex, as found in the negatively charged $SO_2^- \cdot H_2O$ complex from an argon matrix,[70] geometry optimization gave S−O 1.460 Å and OSO 117.6° for the long O···H−O_w distances 3.30 Å and the SO_2 frequencies 1129.7 (ν_1), 1298.9 (ν_3), and 510.9 (ν_2) cm^{-1} (Figure S-4). Thus, even though the magnitude of the effects is smaller in that weakly hydrogen bonded system, the trends on the OSO angle and frequencies are similar to those found experimentally for SO_2(g) and SO_2(aq). Another geometry optimized hydration model (Figure S-4), with three hydrogen-bonding water molecules bridging the SO_2 oxygen atoms, reduced the OSO angle to 118.0° (S−O 1.459 Å).

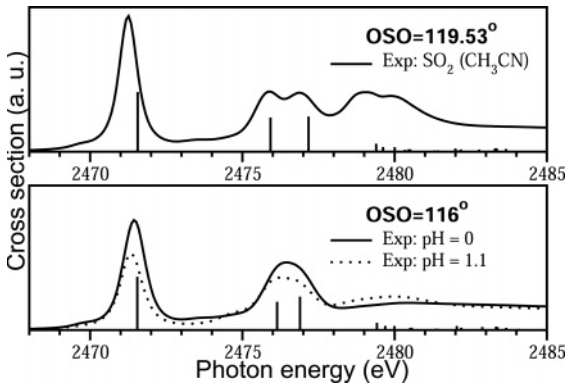

Figure 4. Calculated S(1s) transitions (vertical bars) for the SO_2 molecule (S−O bond distance 1.432 Å) with different OSO angles in C_{2v} symmetry. The experimental XANES spectra are (top) SO_2 dissolved in acetonitrile and (bottom) 0.05 M Na_2SO_3 dissolved in 1 M HCl (pH = 0) and ∼5% SO_2 dissolved in water to pH ≈ 1.1.

Sulfite Solutions. For the aqueous sulfite solution at pH = 3.9 (Figure 3b), the observed features in the experimental spectrum are produced by the two tautomeric ions, sulfonate HSO_3^- and hydrogen sulfite SO_3H^- (Figure 3). The dimerization via an S−S bond to form $S_2O_5^{2-}$ ions that occurs at high concentration[62] can safely be ignored at the relatively low concentration (0.05 M) in this study. At 1 M total sulfite concentration and pH = 4, i.e., the concentration used for the Raman measurements, the concentration of $S_2O_5^{2-}$ is expected to be about 0.2 M.[62]

Theoretical spectra were calculated for the two isomeric HSO_3^- and SO_3H^- ions described in Table 6 to interpret the experimental spectrum and to get an estimate of their relative amounts. C_{3v} symmetry was used for the sulfonate ion, HSO_3^-, with parameters from our neutron diffraction study on solid $CsDSO_3$ (Table S-1). For the SO_3H^- ion no crystal structure is available and the structure was optimized by means of GAUSSIAN98, Table 6, without imposing symmetry restrictions. The hydrogen bonding expected in aqueous solution was simulated by assuming one hydrogen bond at an O···O distance of 2.75 Å from each oxygen atom to a water molecule (Figures 4 and 5), within the range calculated for such hydrogen-bonded O···O equilibrium

(72) Simonov, M. A.; Troyanov, S. I.; Kemnitz, E.; Hass, D.; Kammler, M. *Kristallografiya* **1986**, *31*, 1220−1221.

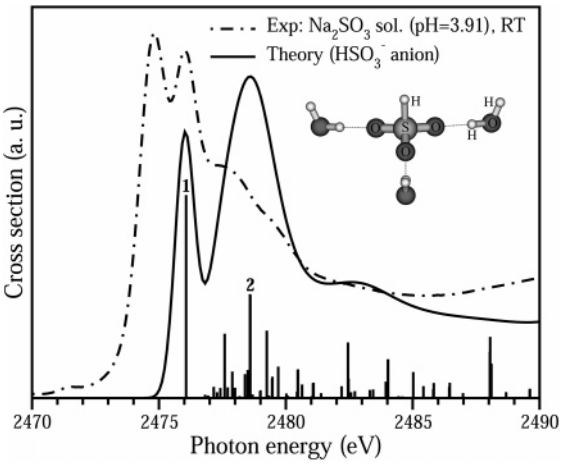

Figure 5. Theoretical S K-edge XANES spectrum (solid line) of the hydrated HSO_3^- ion compared with the experimental XANES spectrum for 0.05 M Na_2SO_3(aq) (dot−dashed line). The minor feature at ∼2471.5 eV corresponds to a small amount of SO_2(aq) present at pH = 3.9 (cf. Figure 3). The vertical bars represent the calculated transition energies and cross sections, convoluted with 0.9 eV FWHM Gaussians below IP = 2476.35 eV, linearly increasing to 8 eV FWHM at and above 2496.35 eV. The unoccupied molecular orbitals corresponding to transitions 1 (LUMO) and 2 are shown in Figure S-3.

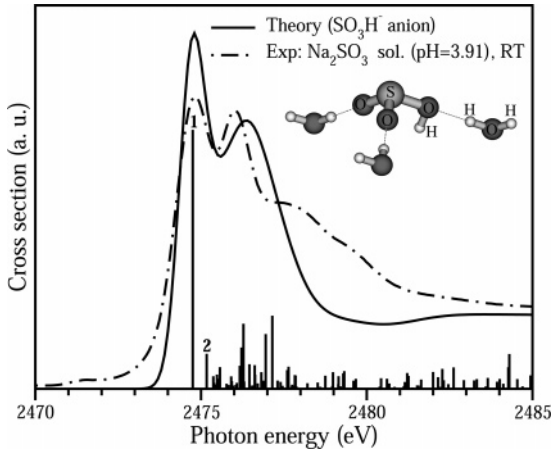

Figure 6. Theoretical S K-edge XANES spectra for SO_3H^- with three hydrogen-bonded water molecules (solid line), compared with the experimental spectrum of 0.05 M Na_2SO_3 in aqueous solution at pH = 3.9 (dot−dashed line). The transitions were convoluted with 0.9 eV FWHM Gaussian functions below 2474.9 eV, linearly increased to 8 eV FWHM after 2494.9 eV.

distances (2.7−2.9 Å).[71] We found the influence on the theoretical spectrum of a variation within this range insignificant.

A recent computational study, describing the mechanism of the transition from hydrated SO_3H^- to HSO_3^- species, showed that the protonated S−O−H group in the SO_3H^- ion is quite sensitive to direct hydrogen-bonded interactions with the sulfur atom.[10] The geometry optimization of the isolated SO_3H^- ion resulted in a very long S−O bond distance (1.826 Å) for the S−O−H group. In the transition state, when a hydrogen atom approached the sulfur atom with an S···H interaction of 1.432 Å, the S−O bond distance of the S−O−H group was reduced to 1.619 Å.[10] The S−O bond distance arrived at in our computation for the protonated S−O−H group was 1.60 Å, while those for the hydrogen-bonded S−O(···H) entities were about 1.51 Å (Table 6). Such a difference is reasonable when considering crystal structures of hydrogen sulfates, HSO_4^-,[72,73] which show about 0.1 Å longer S−O bond distances when protonated. The structural model used to compute the theoretical XANES spectra for the hydrated sulfonate (HSO_3^-) and the hydrogen sulfite (SO_3H^-) ions are shown in Figures 5 and 6, respectively.

The S(1s) transitions calculated for the hydrated HSO_3^- and SO_3H^- ions display a large number of excited states with low transition probability. The first most intense transition 1 around 2475 eV is to the LUMO of A_1 symmetry with excitation from S(1s) into an antibonding σ^*(H−S) molecular orbital. The relaxation energy, −4.05 eV/-3.90 eV for HSO_3^- and SO_3H^-, respectively, calculated for transition 1, was applied to all transitions together with the relativistic shift (+7.4 eV). The transition 2 at 2478.5 eV that is second in intensity is to a doubly degenerate E state and corresponds to excitation into molecular orbitals of mixed character, dominated by bonding π character between S and H together with some antibonding $\sigma^*-\pi^*$ character between the S and O atoms (Figure S-3).

The computed energy for the main transition of the hydrated SO_3H^- ion with 3 hydrogen-bonded water molecules (Figure 6) was found to be sensitive to the S−O(−H) bond distance, which was varied within the range 1.817 to 1.60 Å (Figure S-5). The S−O distance 1.60 Å gave the best agreement. The calculation shows that the first peak in the experimental XANES spectrum for 0.05 M Na_2SO_3(aq) at pH = 3.9, which is generated by two electronic transitions separated by 0.42 eV, can be entirely ascribed to the SO_3H^- ion. The first transition 1 at 2474.8 eV has the highest cross section and corresponds to S(1s) excitation into the antibonding σ^*(O−H) LUMO, while transition 2 is to a local σ^*(O−H) molecular orbital with Rydberg character. The contours of the molecular orbitals 1 and 2 show some charge transfer from sulfur to the oxygen atoms of the hydrogen-bonded water molecules; cf. Figure S-3.

The comparison with the experimental XANES spectrum in Figure 5 shows that the main contribution from the HSO_3^- isomer is to the second experimental XANES peak at 2476 eV and in the region around 2479 eV. The theoretical spectra of the two tautomeric isomers were combined in different proportions with the best fit to the experimental spectrum obtained for the ratio SO_3H^-:HSO_3^- ≈ 72:28, as displayed in Figure 7. The error limit from the fitting procedure is estimated to ±5%. Another error contribution would be systematic differences in the calculated transition moments

(73) Werner, C.; Trojanov, S.; Kemnitz, E.; Worzala, H. *Z. Anorg. Allg. Chem.* **1996**, *622*, 380−384.
(74) Petrucci, R. H. *General chemistry-Principles and modern applications*, 5th ed.; Macmillan Publishing Co.: New York, 1989; p 515.
(75) Polo, S. R.; Wilson, M. K. *J. Chem. Phys.* **1954**, *22*, 900−903.
(76) Evans, J. C.; Bernstein, H. J. *Can. J. Chem.* **1955**, *33*, 1270−1272.
(77) Simon, A.; Waldmann, K. *Z. Phys. Chem.* **1955**, *204*, 235−244.
(78) *Landolt-Börnstein Physikalisch-Chemische Tabellen*; Springer-Verlag: Berlin, 1951; Vol II.
(79) Ross, S. D. *Spectrochim. Acta* **1962**, *18*, 1575−1578.
(80) Bondybey, V. E.; English, J. H. *J. Mol. Spectrosc.* **1985**, *109*, 221−228.
(81) Kaldor, A.; Maki, A. G.; Dorney, A. J.; Mills, I. M. *J. Mol. Spectrosc.* **1973**, *45*, 247−252.

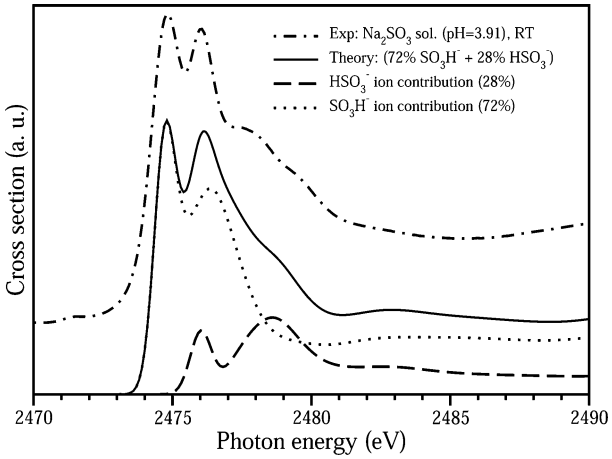

Figure 7. Theoretical S K-edge XANES spectrum for the hydrated SO_3H^- (72%) and HSO_3^- (28%) isomers (solid line) compared with the experimental spectrum of 0.05 M Na_2SO_3 in aqueous solution at pH = 3.9 (dot−dashed line). The separate contribution of each ion is shown below.

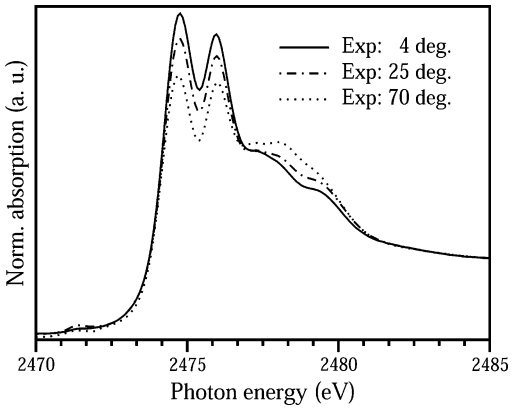

Figure 8. Experimental sulfur K-edge XANES spectra of 0.05 M Na_2SO_3(aq) at pH = 3.9. Temperature variation: 4 °C (solid line); 25 °C (dot−dashed line); 70 °C (dots). The minor feature at ∼2471.5 eV originates from a small amount of SO_2(aq); cf. Figure 3.

calculated as the dipole matrix element between the initial and final state. However, since the resolved XANES features correspond to transitions to well-defined MO's for both tautomeric species, their intensity ratio is not expected to contain appreciable systematic deviations. This is supported by the transition-potential calculation giving near-identical transition moments for the fully relaxed, Δ(Kohn−Sham) corrected LUMO orbitals.

The temperature dependence of the XANES spectra of a 0.05 M Na_2SO_3(aq) solution at pH = 3.9 (Figure 8) shows a reduction of the first two peaks, while the intensity in the 2477−2481 eV region increases with increasing temperature, consistent with a higher relative amount of the HSO_3^- isomer. In summary, our results confirm that the SO_3H^- isomer dominates and that the amount of its tautomer, HSO_3^-, increases with increasing temperature, in qualitative agreement with the NMR results of Horner and Connick.[9]

Sulfite Ion in Solution and in the Solid State. The pyramidal SO_3^{2-} structure from the crystal structure of sodium sulfite (Table 6)[66] was used with the same procedure and basis sets for calculating a theoretical XANES spectrum. For modeling the hydration in aqueous solution, two water molecules were assumed to be directly hydrogen bonded to each sulfite oxygen atom with the O···O distance 2.75 Å and three others positioned above the sulfur atom at the S···O distance 3.5 Å (Figure S-6). To stabilize and distribute the negative (−2) charge, a large number of water molecules was required and the environment was finally extended to encompass 21 water molecules. The computed transition energies remained higher than the corresponding experimental energies even after correcting for the relativistic (+7.4 eV) and relaxation effects. The relaxation shift (−2.90 eV) of the first transition was applied to all states. For the model with merely three hydrogen-bonded water molecules the discrepancy between the energy of the calculated and the experimental main features was about +2.1 eV, which reduced to +1.1 eV for the model with 21 water molecules around the sulfite ion. Further model extensions were deemed impractical, and the energy scale of the final theoretical spectrum was instead shifted (Figure 9).

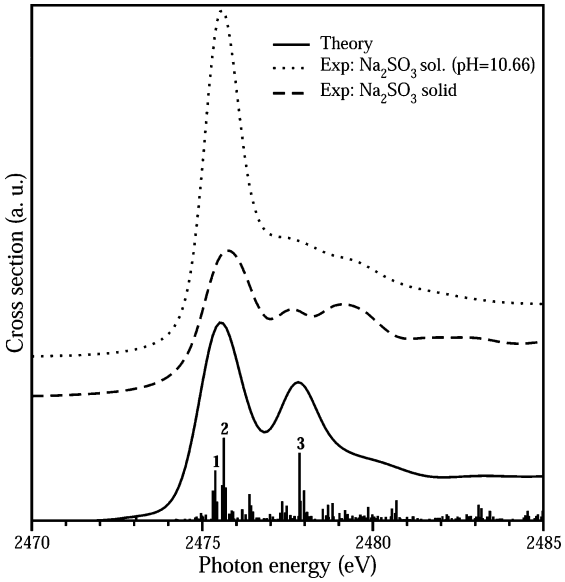

Figure 9. Sulfur K-edge XANES spectra of 0.05 M Na_2SO_3(aq) solution at pH = 10.7 (dots) and solid Na_2SO_3 (dashes) and the theoretical spectrum of the model with 21 water molecules around the sulfite ion (solid line), generated by convoluting the calculated transitions with 1.2 eV FWHM Gaussians below 2475 eV, linearly increasing to 8 eV FWHM at 2495 eV.

The first experimental peak at 2475.8 eV consists of several transitions with the most intense at 2475.4 and 2476.6 eV denoted transitions 1 and 2 in Figure 9. The molecular orbitals corresponding to these transitions display 3p lone pair character on the sulfur atom. Transition 3 at 2477.9 eV with the second highest intensity is attributed to an MO with antibonding σ^* S−O bond character. The transitions 1 and 3 show some charge transfer to the oxygen atoms of the surrounding water molecules (cf. Figure S-3).

XANES of the Solid Sulfonate $CsHSO_3$. The sulfur K-edge XANES spectrum shows one asymmetric broad peak around 2478.1 eV and several resonances at 2481, 2485.7, and 2488 eV (Figure 10), with an appearance rather different from that of the spectrum expected for the hydrated sulfonate ion in solution (cf. Figure 5). The calculated transitions show that the features present at higher energies are transitions into Rydberg states, together with multiple-scattering effects enhanced by the long-range order in the structure. The first

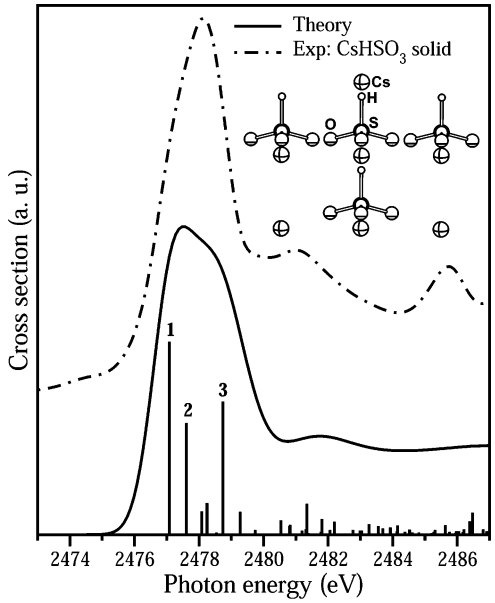

Figure 10. Experimental (dot−dashed line) S K-edge XANES spectrum of crystalline $CsHSO_3$, compared with the calculated spectrum (solid line) for the model in the inset. The convolution of the transitions was performed with 1.35 eV FWHM Gaussian functions below 2477.1 eV, linearly increasing to 8 eV FWHM after 2497.1 eV. The MO's corresponding to transitions 1−3 are illustrated in Figure S-3.

asymmetrical peak could be reproduced fairly well with a model only including the HSO_3^- ion. However, a larger size model was required to describe the shape of the resonances. Four HSO_3^- units and seven cesium cations were introduced around the central core-excited sulfur atom, keeping C_{3v} symmetry; cf. Figure 10 (atomic coordinates in Table S-8). The relaxation effect of the first state (−3.82 eV) was applied as an overall shift to all the states together with the relativistic shift (+7.4 eV).

The first three transitions are to MO's belonging to the A_1 symmetry species of the C_{3v} point group, followed by one transition into an E state, one A_1, and then another two E states. The first two transitions of A_1 symmetry, 1 and 2, at 2477.1 and 2477.6 eV, respectively, are to the LUMO and LUMO+1, while the second highest intensity transition 3 at 2478.7 eV (E) is into LUMO+6 and LUMO+7, respectively; cf. Figure 10. The first two A_1 states are transitions into MO's with antibonding σ^*(S−O) and σ^*-(H−S) bond character, while the doubly degenerate E state 3 is attributed to molecular orbitals with dominating bonding π character between the H and S atoms and mixed antibonding $\sigma^*-\pi^*$ (S−O) bond character.

XANES of Substituted $X_3CSO_3^-$ Sulfonates. The above experimental XANES spectrum of the sulfonate ion in $CsHSO_3$ shows significant influence from the regular nonbonded surrounding in the crystalline solid. However, the intramolecular effects can be greater and more specific, as was found when substituting the hydrogen atom with groups of different bonding character in the $X_3CSO_3^-$ ions with X = H, Cl, and F (cf. Figure 11). The main absorption peak is fairly similar in the experimental spectra of the $CsHSO_3$ and $NaCH_3SO_3$ compounds. Both the HSO_3^- and $CH_3SO_3^-$ ions have C_{3v} point group symmetry with similar character of the S−H and S−CH_3 bonds[63] and with similar S−O bond

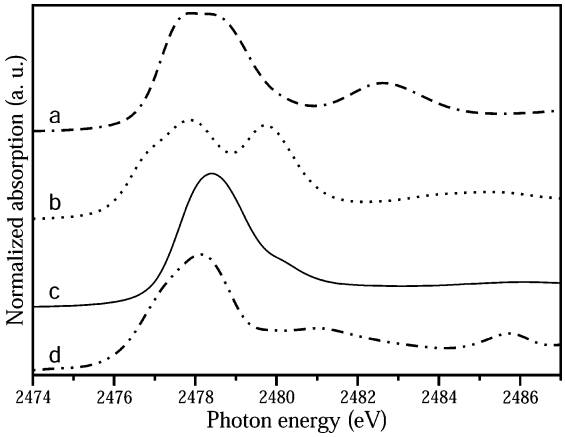

Figure 11. Experimental S K-edge XANES spectra of the following solid compounds: (a) sodium trifluoromethanesulfonate, $NaCF_3SO_3$; (b) sodium trichloromethanesulfonate hydrate, $NaCCl_3SO_3{\cdot}H_2O$; (c) sodium methanesulfonate, $NaCH_3SO_3$; (d) cesium sulfonate, $CsHSO_3$.

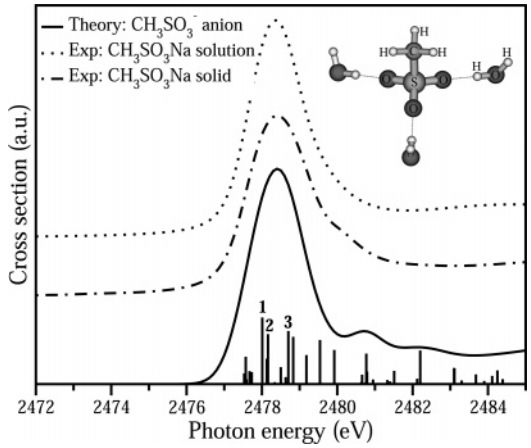

Figure 12. S K-edge XANES spectra of sodium methanesulfonate in 0.05 M aqueous solution (dots) and in the solid state (dot−dashed line). The theoretical spectrum (solid line) is obtained by convoluting the vertical bars with 1.1 eV FWHM Gaussian functions below 2476.2 eV, increasing to 8 eV FWHM after 2496.2 eV. The transitions 1−3 are to MO's of A_1, E, and E symmetry, respectively (Figure S-3).

distances (Table 4). When there is substitution of the hydrogen atoms in the methyl group with chlorine or fluorine, significant changes occur both for aqueous solutions (0.05 M) and the solid-state S K-edge XANES spectra of sodium trichloromethanesulfonate monohydrate, $NaCCl_3SO_3{\cdot}H_2O$, and sodium trifluoromethanesulfonate, $NaCF_3SO_3$.

Theoretical spectra were obtained in a similar way as above (Table 6) for the $X_3CSO_3^-$ (X = H, Cl, F) anions in staggered C_{3v} conformation,[33,39,41] with the hydration simulated by assuming one water molecule hydrogen bonded to each oxygen atom, and compared with the corresponding solution and solid-state experimental spectra in Figures 12−14, respectively. For the hydrated $CH_3SO_3^-$ anion, the corrections to the calculated transition energies were obtained by applying the separately calculated relaxation effects for the first 9 A_1 and 7 E states and shifting the remaining states with the mean value (−4.04 eV). In addition to the relativistic effect (+7.4 eV), the theoretical spectrum was shifted +0.5 eV as a remaining effect of the charge distribution. Also, the spectra of the related anions, trichloromethanesulfonate and trifluoromethanesulfonate, were shifted similarly +0.5

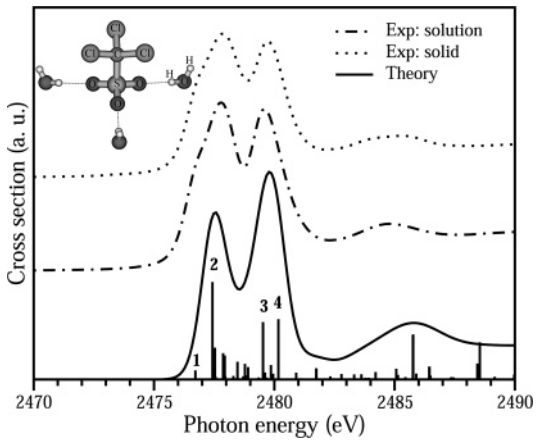

Figure 13. Sulfur K-edge XANES spectra of $NaCCl_3SO_3 \cdot H_2O$ in the solid state (dots) and in 0.05 M aqueous solution (dot−dashed). The theoretical spectrum (solid line) was obtained by convoluting the calculated transitions (vertical bars) with 1.1 eV FWHM Gaussian functions below 2476.5 eV, linearly increased to 8 eV FWHM after 2496.5 eV. The transitions 1 and 2 are to MO's of A_1 symmetry, while transitions 3 and 4 are to E states.

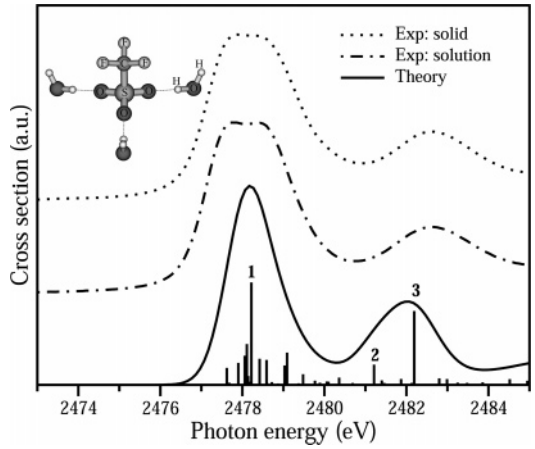

Figure 14. Sulfur K-edge XANES spectra of $NaCF_3SO_3$ in the solid state (dots) and in 0.05 M aqueous solution (dot−dashed). The theoretical spectrum (solid line) for the symmetrical model in the inset was obtained by convoluting the calculated transitions with 1.1 eV FWHM Gaussian functions below 2476.7 eV, linearly increased to 8 eV FWHM after 2496.7 eV. Transition 1 is to an unoccupied MO of A_1 symmetry, while transitions 2 and 3 are to doubly degenerate E states.

eV. Several strong transitions contribute to the main experimental peak at 2478.4 eV, and the most intense are specified in Figure 12. Transition 1 at 2478 eV is into an antibonding σ^*(S−C) MO of A_1 symmetry. The E states 2 and 3 at 2478.2 and 2478.7 eV correspond to transitions into molecular orbitals of π(S−C) bonding and antibonding π^*(S−O) character, respectively (Figure S-3).

The main experimental features in the XANES spectra of the trichloromethanesulfonate ion, at about 2477.9 and 2479.7 eV with a shoulder at 2476.8 eV both in the solid state and aqueous solution, are fairly well reproduced by the calculated transitions (Figure 13). Separate relaxation effects were evaluated and applied to the first 8 A_1 and 7 E states and their mean value (−3.90 eV) was applied to the remaining transitions, in addition to the relativistic (+7.4 eV) and charge distribution shifts (+0.5 eV). The 2477.9 eV peak has contributions from several components. Transition 2 with the highest cross section is assigned as an excitation from S(1s) into the antibonding σ^*(C−S) LUMO+4 of A_1 symmetry at 2477.4 eV. Also the transition 1 to the LUMO (A_1) with lower intensity at 2476.7 eV has antibonding σ^*-(C−Cl) character. The second main experimental peak at about 2479.7 eV is also composite with its main transitions 3 and 4 attributed to two doubly degenerate E states separated by 0.66 eV in the calculations. The first E state involves an excitation to an antibonding σ^*(S−O) MO, while the second has local antibonding π^*(C−S) character (Figure S-3). The resonance at 2485.3 eV is fairly well reproduced by the calculations.

For the trifluoromethanesulfonate ion, both in the solid state and in solution, the experimental XANES spectra show a main broad composite peak, 2478−2479 eV, and an additional broad feature at 2482.6 eV. In the model calculations separate relaxation effects were applied to the first 5 A_1 and 3 E states and their mean value (−4.09 eV) was applied to the remaining states, as well as the overall relativistic (+7.4 eV) and charge distribution shifts (+0.5 eV), resulting in a theoretical XANES spectrum where the main features are reproduced, Figure 14. However, the C_{3v} model used could not fully generate the unresolved broadening of the main peak, which probably is due to instantaneous vibrational asymmetry. The effect of asymmetry on the spectra was tested by calculating theoretical spectra for the four crystallographically independent configurations of the trifluoromethanesulfonate ions in anhydrous sodium trifluoromethanesulfonate (Figure S-7).[39] The distribution of S−O distances and OSO angles resulted in electronic states with somewhat different energies and intensities.

As for the trichloromethanesulfonate ion the strongest calculated transition 1 at 2478.2 eV is ascribed to an antibonding (C−S) σ^* MO of A_1 symmetry. The main contribution to the experimental peak at 2482.6 eV is given by the doubly degenerate E state denoted 3, which has (C−S) antibonding π^*-character, as well as another E state denoted 2, Figure 14. The electronegative CF_3 group significantly reduces the electron population on the carbon atom, especially for the p-electrons (Table 5). This delocalization probably causes the energy shifts with several eVs to high energy of the XANES absorption features of π^* character for the unoccupied E state MO's 2 and 3.

Conclusions

Sulfur K-edge XANES spectra are informative for studying sulfur species, in particular in combination with DFT transition potential calculations. The excellent agreement, especially for neutral molecules between absolute calculated and experimental energies and energy separations allows description and assignment of the S(1s) transitions to the unoccupied valence molecular orbitals. The distinctly different spectra for aqueous sulfite(IV) solutions with pH values about 0, 4, and 11 have been investigated. Hydrated molecular sulfur dioxide, SO_2(aq), was confirmed to be the only detectable sulfur(IV) species at low pH (<1). The preedge experimental features in the XANES spectra of the SO_2 molecule in gas phase and acetonitrile solution are satisfactorily explained by the theoretically calculated XANES

spectrum with good agreement between calculated and experimental transition energies. The first transition is to the totally antibonding π_g* LUMO. The separation between the following transitions at higher energy to LUMO+1 and LUMO+2, which involve the oxygen 2p atomic orbitals, depends on the OSO angle, which is found to decrease because of the hydration in aqueous solution. The decrease of about 3° is consistent with an OSO angle of ~116° for the SO_2(aq) molecule, implying fairly strong hydrogen bonding.

The equilibrium and temperature variation between the two coordination isomers, the sulfonate (HSO_3^-) and hydrogen sulfite (SO_3H^-) ions with the hydrogen atom coordinated to sulfur and oxygen, respectively, was studied in sulfite solutions with pH ~4. The S(1s) electron transitions were interpreted by the DFT−TP method, and theoretical spectra were calculated for both isomers. The best description of the experimental S(1s) XANES spectrum at ambient temperature was found by combining the calculated spectra in the ratio SO_3H^-:HSO_3^- ≈ 0.72:0.28. Temperature variation showed that the relative amount of sulfonate increased at increasing temperature, even though the SO_3H^- species still dominates. The equilibrium quotient at 298 K, Q_d = [SO_3H^-]:[HSO_3^-] = 2.6 ± 0.5, obtained in this work from the ratio of the two isomers at the total concentration of 0.05 M without ionic medium, is smaller than the previously reported value obtained by means of ^{17}O NMR, Q_d = 4.9 ± 0.1, at 1.0 m ionic strength.[9] For the hydrated sulfite (SO_3^{2-}) ion that dominates at high pH, a model allowing adequate charge distribution was found to be important for the theoretical description.

The crystal structure of $CsDSO_3$ was determined from neutron powder diffraction data. For the sulfonate ion in C_{3v} symmetry the S−D and S−O bond distances 1.38(2) and 1.44(1) Å, respectively, were obtained. The influence on the S(1s) transitions of the surrounding matrix was evaluated for the solid $CsHSO_3$ compound. Pronounced solid-state effects were found for the cesium sulfonate $CsHSO_3$, where transitions into Rydberg states, together with multiple-scattering effects, enhanced features near the absorption edge. By similar studies on the $NaCH_3SO_3$, $NaCCl_3SO_3{\cdot}H_2O$, and $NaCF_3SO_3$ compounds in solution and in the solid state, combined with force field analyses of the vibrational spectra, the intramolecular effect on the electron distribution by the CX_3 groups for X = H, Cl, and F could be analyzed. The main peaks in the HSO_3^- and $CH_3SO_3^-$ spectra are of similar shape and energy, while new higher energy features appear in the XANES spectra for trichloromethanesulfonate and trifluoromethanesulfonate with the electronegative CCl_3 and CF_3 groups, respectively. The steric repulsion in the $Cl_3CSO_3^-$ ion has profound effects on both vibrational and XANES spectra. The electron-withdrawing effect especially of the CF_3 group in $CF_3SO_3^-$ delocalizes the S−O π-bonds, lowers the S−O, and increases the CS force constants in comparison with those of the $Cl_3CSO_3^-$ ion. A broadening of the main sulfur XANES spectral feature for $F_3CSO_3^-$ may be a result from the change in S−O bond character promoting larger instantaneous asymmetry in the $-SO_3$ group. The large decrease of the p-electron population at the carbon atom probably causes transitions to E state molecular orbitals of π* symmetry to shift significantly.

The formal oxidation state of all the sulfur species in Table 5 is S^{IV}, even though Mulliken population analyses show a two-electron charge difference for the sulfur atom between the sulfite SO_3^{2-} and the $CF_3SO_3^-$ ions (Table 5). The XANES spectra of, e.g., the SO_2 molecule and the $F_3CSO_3^-$ ion show an energy difference of several eV between their first electronic transitions (cf. Figures 3, 4, and 11). Because each transition of the S(1s) electron to an unoccupied molecular orbital occurs within the same potential, the transition energy, which is the energy difference between the orbital energies, should not be much influenced by the sulfur ionicity. However, the population analysis indicates a change in the electron distribution between the molecular orbitals, whereas the change in the atomic charge indicates a change in the type of bonding, which evidently influences the energies of the unoccupied molecular orbitals.

Acknowledgment. The financial support by the Swedish Science Research Council and the allocation of beam-time and laboratory facilities by the SSRL made this study possible. The SSRL is operated by the Department of Energy, Office of Basic Energy Sciences. The SSRL Biotechnology Program is supported by the National Institutes of Health, National Center for Research Resources, Biomedical Technology Program, and by the Department of Energy, Office of Biological and Environmental Research. We are grateful to Dr. Farideh Jalilehvand for assistance with the experimental XANES data treatment and to Dr. Serena DeBeer George and Dr. Eileen Yu Sneeden, SSRL, for assistance with the XANES measurements and for providing the gas-phase spectra of sulfur dioxide. Dr. Mikhail Maliarik, Linköping University, kindly assisted with the Raman measurements on aqueous solutions.

Supporting Information Available: Table S-1, listing the atomic coordinates and the isotropic temperature parameter (B_{iso}) obtained from the Rietveld refinement on crystalline $CsDSO_3$ from neutron powder diffraction data, Tables S-2 and S-5, containing observed and calculated frequencies with assignments and the potential energy distribution for HSO_3^- and DSO_3^- (Table S-2) and $CH_3SO_3^-$, $CCl_3SO_3^-$, and $CF_3SO_3^-$ (Table S-5), Tables S-3 and S-4, containing complete spectra, including overtones and binary combination bands with assignments, for $CsHSO_3$/$CsDSO_3$ and $NaCH_3SO_3$/$NaCCl_3SO_3{\cdot}H_2O$, Table S-6, including the vibrational DFT-calculated frequencies for all the investigated species except the sulfite ion, Table S-7, showing calculated/observed frequencies with assignments for $S^{16}O_2$, $S^{18}O_2$, and $S^{16}O^{18}O$, SO_3, and SO_3^{2-} and SO_4^{2-} species, Table S-8, listing atomic coordinates for the XANES model of solid $CsHSO_3$, Figure S-1, displaying observed and calculated neutron diffraction patterns for $CsDSO_3$, Figure S-2, showing the correlation between SO−SO bond interaction force constants and separations between asymmetric and symmetric SO_3 stretching frequencies, Figure S-3, illustrating contours of the molecular orbitals for the transitions marked in the calculated XANES spectra for the species SO_2, HSO_3^-, SO_3H^-, SO_3^{2-}, solid $CsHSO_3$, $CH_3SO_3^-$, $CCl_3SO_3^-$, and $CF_3SO_3^-$, Figure S-4, comparing the transition energies and intensities calculated for the SO_2 molecule with a constant S−O bond distance (1.432

Å) and different OSO angles (110, 113, 115, 115.5, 116, 117, and 119.53°), Figure S-5, comparing the theoretical S K-edge XANES spectra for SO_3H^- ion hydrated with three water molecules having different S−O(−H) bond distances, Figure S-6, displaying the model used to compute the theoretical XANES spectrum of the hydrated sulfite anion, and Figure S-7, illustrating the theoretical K-edge XANES spectra calculated for four different asymmetric configurations of the triflate ion, as reported for anhydrous sodium triflate. This material is available free of charge via the Internet at http://pubs.acs.org.

IC062440I